Prediction of the Temperature Distribution in Asphalt Pavement Samples

by

Marco Burger

Thesis presented at the University of Stellenbosch in partial fulfilment of the requirements for degree of

Master of Mechanical Engineering

Department of Mechanical Engineering
University of Stellenbosch
Private Bag X1
Matieland
South Africa
7602

Study Leader: Prof D.G. Kröger

April 2005

Declaration

I, the undersigned, hereby declare that the work contained in this thesis is my own original work and that I have not previously in its entirety or part submitted it at any university for a degree.

Signature:

M. Burger

Date:

Abstract

Prediction of the Temperature Distribution in Asphalt Pavement Samples

M. Burger

Department of Mechanical Engineering
University of Stellenbosch
Private Bag X1, Matieland, South Africa, 7602

Thesis: MScEng (Mechanical)

April 2005

The convection heat transfer coefficient between an infinite, horizontal surface and the natural environment is determined experimentally. It is shown that, during daytime, heat is transferred due to natural and forced convection, while during nighttime heat is transferred due to conduction and forced convection. Equations that correlate the daytime and nighttime convective heat transfer coefficients respectively, are presented. The results are compared with values obtained by other investigators.

The equations for the convection heat transfer coefficient are then used to predict the surface temperature and the temperature at depth of asphalt pavement samples using a simulation model. It is found that there is good agreement between the measured and the predicted asphalt pavement sample temperatures.

Opsomming

Voorspelling van die Temperatuurverdeling in Asfalt-padoppervlakmonsters

M. Burger

Departement van Meganiese Ingenieurswese
Universiteit van Stellenbosch
Privaatsak X1, Matieland, Suid-Afrika, 7602

Tesis: MScIng (Meganies)

April 2005

Die konveksie warmteoordrags-koëffisiënt tuseen 'n oneindige, horisontale oppervlak en die natuurlike omgewing is eksperimenteel bepaal. Daar word getoon dat warmte, tydens die dag, oorgedra word deur natuurlike en geforseerde konveksie, terwyl warmte tydens die nag oorgedra word deur geleiding en geforseerde konveksie. Die resultate word vergelyk met die resultate van ander navorsers. Vergelykings wat die konveksie warmteoordrags-koëffisiënt gedurende die dag en nag onderskeidelik korreleer word voorgestel.

Die vergelykings vir die konveksie wamteoordrags-koëffisiënt word dan gebruik in 'n simulasiemodel om die oppervlaktemperatuur en die temperatuur onder die oppervlakte van asfalt-padoppervlakmonsters te voorspel.

Acknowledgements

I want to thank my parents and friends for everything they have done for me during this study.

I would also like to thank Prof. Kröger for the opportunity he gave me to do this thesis.

Most of all I want thank my Father in Heaven for His guidance.

Contents

List of Figures

List of Tables

Nomenclature

A	Area, m^2
a	Constant
B	Constant
b	Constant
C_f	Friction coefficient
c	Constant
c_p	Specific heat, J/kgK
D	Diameter, m
d	Depth, m
dt	Time step size, s
EOT	Equation of time, minutes
g	Gravitational acceleration, m/s^2
H	Height, m
h	Convection heat transfer coefficient, W/m^2K
I	Solar radiation, W/m^2
i	Time step, s
k	Thermal conductivity, W/mK
l	Thickness, m
L_{loc}	Location longitude, °
L_{st}	Standard meridian, °
m	Mass, kg

Nu Nusselt number, $\frac{hL}{k}$

n Day of the year or coordinate

p Pressure, N/m^2

Q Electrical power, W

q Energy per unit area, W/m^2

R Electrical resistance, Ω or Gas constant

Ra Rayleigh number, $\frac{g(T_s - T_a)c_p k^2 \rho^2}{\mu T_m}$

sat Saturation

T Temperature, °C or K

t Time, s

V Voltage, V or Volume, m^3

v Speed, m/s

z Coordinate or distance, m

Greek symbols

α Solar absorptivity or diffusivity, m^2/s

ε Emissivity

$\Delta\varepsilon$ Emissivity correction

θ Angle, ° or direction, ° from north

σ Stefan-Boltzmann constant

ρ Density, kg/m^3

μ Dynamic viscosity, kg/ms

Φ Latitude, °

ϕ Relative humidity, %

δ Declination angle, °

ω Hour angle, °

τ Transmission coefficient

Subscripts

a Ambient Air

b	Beam
cond	Conduction
conv	Convection
d	Diffuse or depth
dp	Dew point
e	Effective
fc	Forced convection
g	Ground
h	Hemispherical
L	Length
lw	Long wave
m	Mean
n	Normal
p	Pressure
rad	Radiation
s	Surface or solar
sky	Sky
t	Time
v	Vapour
w	Wind
z	Zenith

Chapter 1 Introduction

Asphalt pavements are exposed to great strains and stresses. During winter cracks can arise due to frost or shrinkage during periods of low temperatures. In summer when solar radiation and air temperatures are high, the pavement becomes softer and there is a risk that heavy vehicles may cause rutting due to plastic deformation.

Various methods have been proposed to predict temperatures in pavements exposed to the natural environment. Solaimanian and Kennedy (1993) developed a method to predict the maximum temperature profile on the basis of maximum air temperature and hourly solar radiation. In most cases studied they claimed that they were able to predict pavement temperatures to within 3 °C.

In the U.S.A a binder and mixture specification for pavement design, Superpave (1994) was developed under the Strategic Highway Research Program (SHRP) to determine among others the highest and lowest pavement surface temperatures with the use of simplified empirical equations. This approach has also found applications, with various degrees of success, in countries outside the U.S.A. like South Africa and Sweden.

Hermansson (2004) developed a relatively extensive simulation model to calculate pavement temperatures for both summer and winter conditions. Although his approach gives good results in many cases, measurable discrepancies do occur in certain locations and at different times during the year. These discrepancies could in part be due to inaccurate heat transfer coefficients.

In the abovementioned and other studies to date certain simplifying assumptions are made and the reliability of some of the heat transfer equations are questionable.

It is the objective of this study to obtain reliable heat transfer equations and to refine existing evaluation methods to predict pavement temperatures more accurately under relatively well-defined environmental conditions. Further future refinement taking into consideration more complex environmental conditions are envisaged. Although a more detailed method of analysis implies more complexity, improved heat transfer equations and a better understanding of the fundamentals involved which are essential before meaningful simplifications can be made. In this study the convection heat transfer of a surface exposed to the natural environment will be studied.

A systematic approach will be followed in this study, ultimately leading to the prediction of the temperature distribution in asphalt pavement samples. Firstly a correlation for the clear sky emissivity will be presented for the use in determining the long wave radiation heat transfer between a surface and the environment, as there are numerous discrepancies between existing correlations. In chapter 3 a correlation for the convection heat transfer coefficient for a surface that is warmer than the ambient air will be presented and in chapter 4 a correlation for a surface that is colder than the ambient air will be presented. In the final chapter the equation for the long wave radiation from the sky and the two correlations for the convection heat transfer coefficients will be used in a simulation model to predict the surface temperature and temperature at depth of a pavement and compared with experimental results.

Chapter 2 Determination of the Clear Sky Emissivity

In this chapter the clear sky emissivity is determined experimentally and a correlation for the calculation of the clear sky emissivity is recommended. In the following chapters the clear sky emissivity will be used to calculate the long wave radiation exchange between a horizontal surface and the environment.

2.1 Introduction and Literature Review

Particles in the atmosphere like dust and smoke and molecules like carbon dioxide, water and ozone not only absorb solar radiation but also radiation from the earth's surface. Predicting the radiative energy exchange between the earth's surface and the atmosphere is very important in determining the performance of solar collectors and greenhouses and the radiative cooling of surfaces like buildings and pavements.

The radiation from the sky can be approximated as a fraction of blackbody radiation corresponding to the temperature of the air near the ground, as given by Mills (1995), i.e.

$$q_{sky} = \sigma T_{sky}^{4} = \varepsilon_{sky} \sigma T_a^{4} \tag{2.1}$$

where σ is the Stefan-Boltzmann constant (5.67×10^{-8} W/m^{2}K^4), T_{sky} is the effective clear sky temperature, ε_{sky} is the clear sky emissivity and T_a is the ambient air temperature near the ground. The sky emissivity ε_{sky} is dependent on the amount of moisture in the air and for this

reason is generally expressed as a linear function of the dew point temperature T_{dp} (in °C) near the surface and the most commonly used correlations are the following:

$$\varepsilon_{sky} = 0.8004 + 0.00396T_{dp} \quad \text{(Bliss (1961))} \tag{2.2}$$

$$\varepsilon_{sky} = 0.787 + 0.0028T_{dp} \quad \text{(Clark and Allen (1978))} \tag{2.3}$$

$$\varepsilon_{sky} = 0.770 + 0.0038T_{dp} \quad \text{(Berger, Buriot and Garnier (1984))} \tag{2.4}$$

$$\varepsilon_{sky} = 0.754 + 0.0044T_{dp} \quad \text{(Tang, Etzion and Meir (2004))} \tag{2.5}$$

Berdahl and Fromberg (1982) recommend the following equation for the clear sky emissivity during nighttime

$$\varepsilon_{sky} = 0.741 + 0.0062T_{dp} \tag{2.6}$$

and

$$\varepsilon_{sky} = 0.727 + 0.0060T_{dp} \tag{2.7}$$

for the clear sky emissivity during daytime.

Martin and Berdahl (1984) expressed ε_{sky} as a quadratic function of dew point temperature, i.e.

$$\varepsilon_{sky} = 0.711 + 0.0056T_{dp} + 0.000073T_{dp}^{2} \tag{2.8}$$

A diurnal correction $\Delta\varepsilon_t$ was added to correct equation (2.8) for use at a particular time of day, i.e.

$$\Delta\varepsilon_t = 0.013\cos\left[2\pi\frac{t}{24}\right] \tag{2.9}$$

where t is the time in hours.

A pressure correction $\Delta\varepsilon_p$ was also added to correct for the observer's elevation, i.e.

$$\Delta\varepsilon_p = 0.00012(p_a - 1000) \tag{2.10}$$

where p_a is the atmospheric pressure in millibar.

Another way of correlating T_{sky} is given by Swinbank (1963):

$$T_{sky} = 0.0552T_a^{1.5} \tag{2.11}$$

This correlation for T_{sky}, based only on ambient air temperature T_a (in K), is however not accurate as the sky temperature changes with the humidity of the air.

2.2 Analysis

Consider the energy balance that is applicable to a unit area of horizontal surface that is exposed to the natural environment on a clear, dry, night, as shown in figure 2.1, i.e.

$$\begin{aligned} h\,(T_a - T_s) &= (\varepsilon\sigma T_s^4 - \alpha_{lw}\sigma\, T_{sky}^4) - k_g(\mathrm{d}T/\mathrm{d}z) \\ q_{conv} &= q_{rad} + q_{cond} \end{aligned} \tag{2.12}$$

where $h(T_a - T_s)$ is the convective heat transfer between the ambient air and the surface.

The first term on the right-hand side of equation (2.12) represents the net long wave radiation between the surface and the atmosphere. The second term on the right-hand side of equation (2.12) represents the heat that is conducted through the ground. If the surface is insulated, this term is negligible.

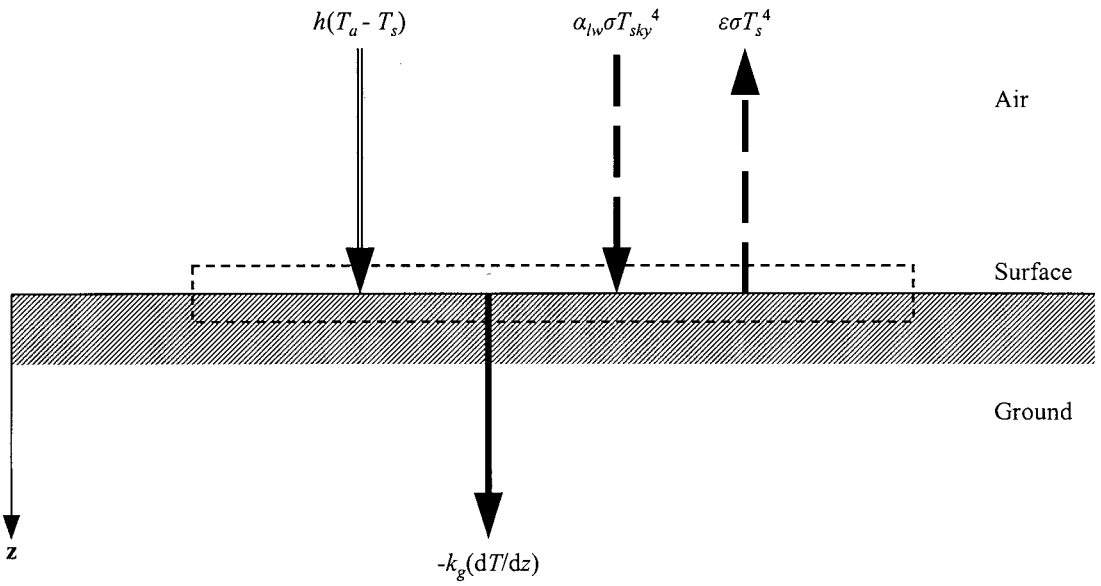

Figure 2.1: Heat fluxes at ground surface exposed to the environment during nighttime.

If an insulated surface is heated by an external source of energy q such that the surface temperature is equal to the ambient air temperature, there will be no convection heat transfer and equation (2.12) becomes

$$q = (\varepsilon\sigma T_s^4 - \alpha_{lw}\sigma\, T_{sky}^4) \tag{2.13}$$

From equation (2.13) it follows that the Kelvin sky temperature is given by

$$T_{sky} = \left(\frac{\varepsilon\sigma T_s^4 - q}{\alpha_{lw}\sigma} \right)^{1/4} \tag{2.14}$$

By rearranging equation (2.1) one can then calculate the nighttime clear sky emissivity ε_{sky} from equation (2.14), i.e.

$$\varepsilon_{sky} = \left(\frac{T_{sky}}{T_a} \right)^4 = \frac{\varepsilon\sigma T_s^4 - q}{\alpha_{lw}\sigma T_a^4} \tag{2.15}$$

2.3 Experimental Set-up and Procedures

Experiments were conducted at the Solar Energy Laboratory of the University of Stellenbosch, Stellenbosch, South Africa (Altitude 100 m, Latitude –33.93 °, Longitude 341.15 ° west). The experimental apparatus, as seen in figure 2.2, consisted of a 1 m × 1 m aluminium plate having a thickness of 5 mm that was painted matt black.

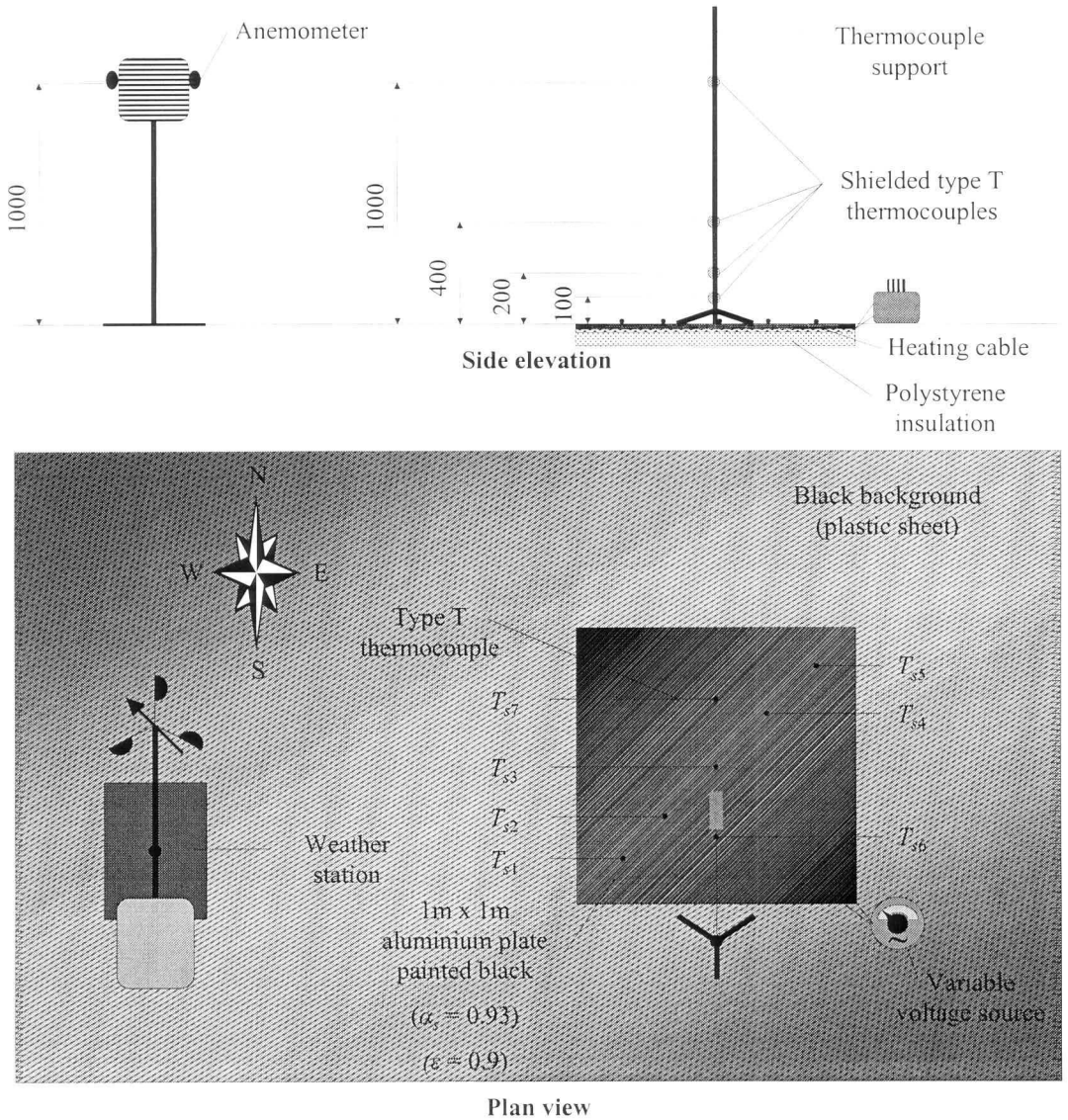

Figure 2.2: Schematic of the experimental set-up.

The solar absorptivity α_s of the black painted surface is taken as 0.93 (Modest (1993)), while the long wave emissivity ε and absorptivity α_{lw} is taken as 0.90 (Mills (1995)). The plate was heated from below with the aid of an underfloor heating cable having a known electrical

resistance R of 88.6 Ω. The lower surface of the aluminium plate was insulated with a 50 mm polystyrene layer. The heating cable was connected to a variable voltage source, which was used to vary the plate temperature.

The surface temperature measurements were obtained from seven type T thermocouples that were embedded on the surface of the plate. Another four type T thermocouples were placed at different heights above the plate to measure the temperature distribution above the plate. All the thermocouples were placed in a bucket of water to see that they measure the same temperature as to assure their measuring accuracy.

A weather station was used to measure ambient air temperature, dew point temperature, barometric pressure, humidity, wind speed and wind direction 1 m above the surface. The anemometers had an accuracy of ± 0.2 m/s, while the temperature sensors had an accuracy of ± 0.1 °C.

The power Q, that was needed to heat the aluminium plate to the ambient air temperature, was calculated by using the equation for electrical power, i.e.

$$Q = V^2/R = qA = q \times 1 = q \tag{2.16}$$

where V is the voltage drop over the heating cable and A is the 1 m^2 surface area of the aluminium plate. The resistance R of the heating cable stayed constant over the measured temperature range.

2.4 Results and Discussion

Figure 2.3 shows an example of the measured surface T_s, ambient air T_a and dew point temperature T_{dp} as a function of solar time during a particular clear night. The power Q was controlled such that T_s is as close as possible to T_a.

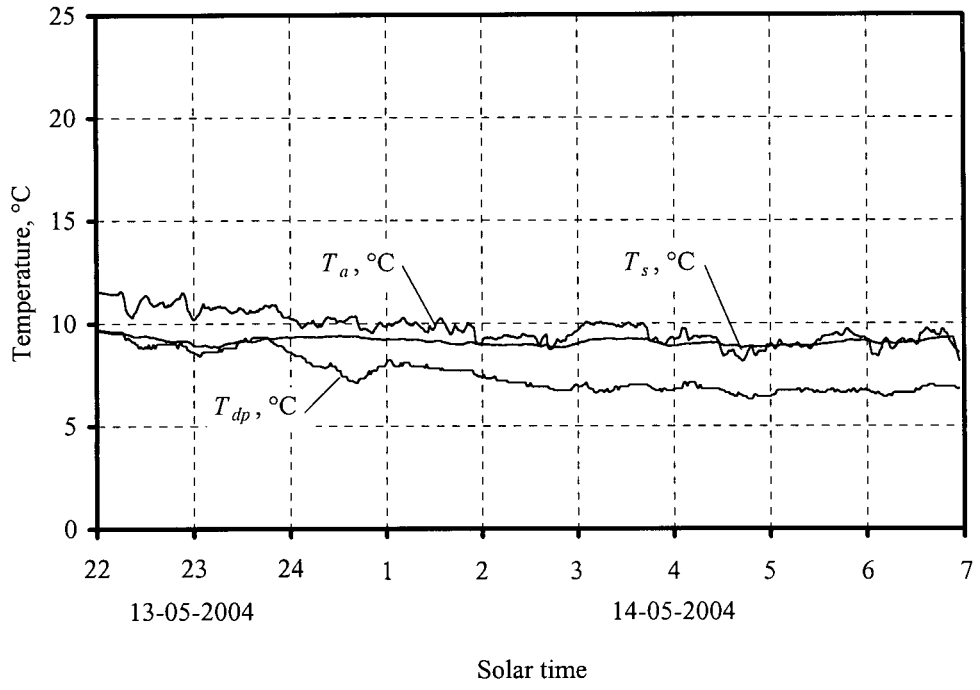

Figure 2.3: Measured surface, ambient air and dew point temperature.

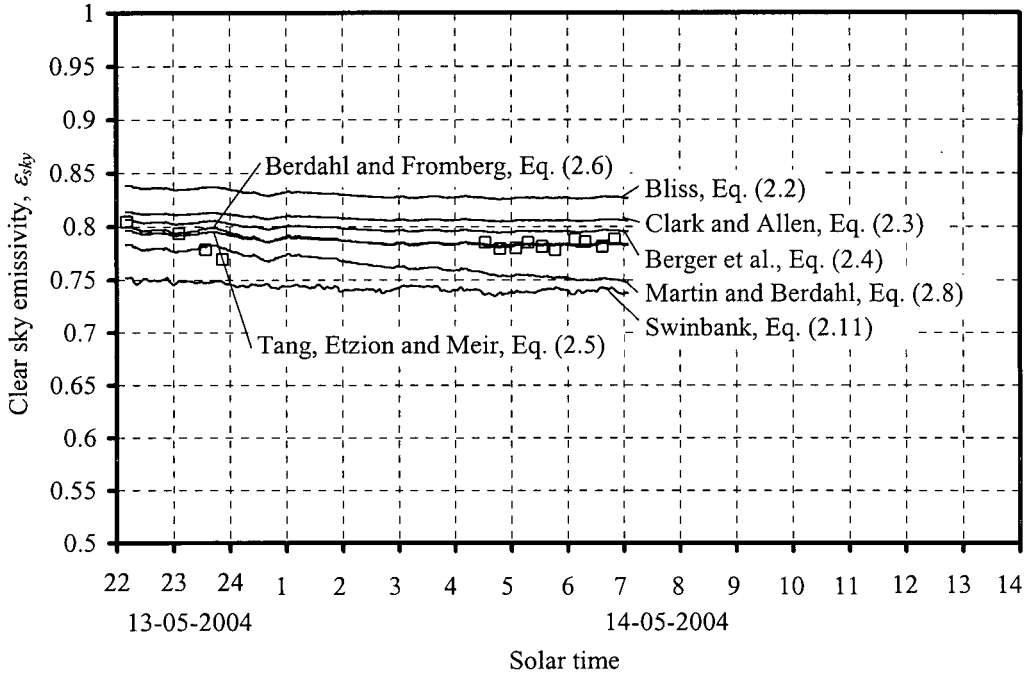

Figure 2.4: Measured and calculated nighttime clear sky emissivity during a particular night.

In figure 2.4 the nighttime clear sky emissivity calculated according to equation (2.15) is shown together with the clear sky emissivity calculated according to equations (2.2) to (2.6), equation (2.8) with diurnal $\Delta\varepsilon_t$ and pressure correction $\Delta\varepsilon_p$ and equation (2.11).

The correlations for the clear sky emissivity given in equations (2.2) to (2.6) and (2.8) is shown in figure 2.5 together with the measured experimental data as a function of dew point temperature.

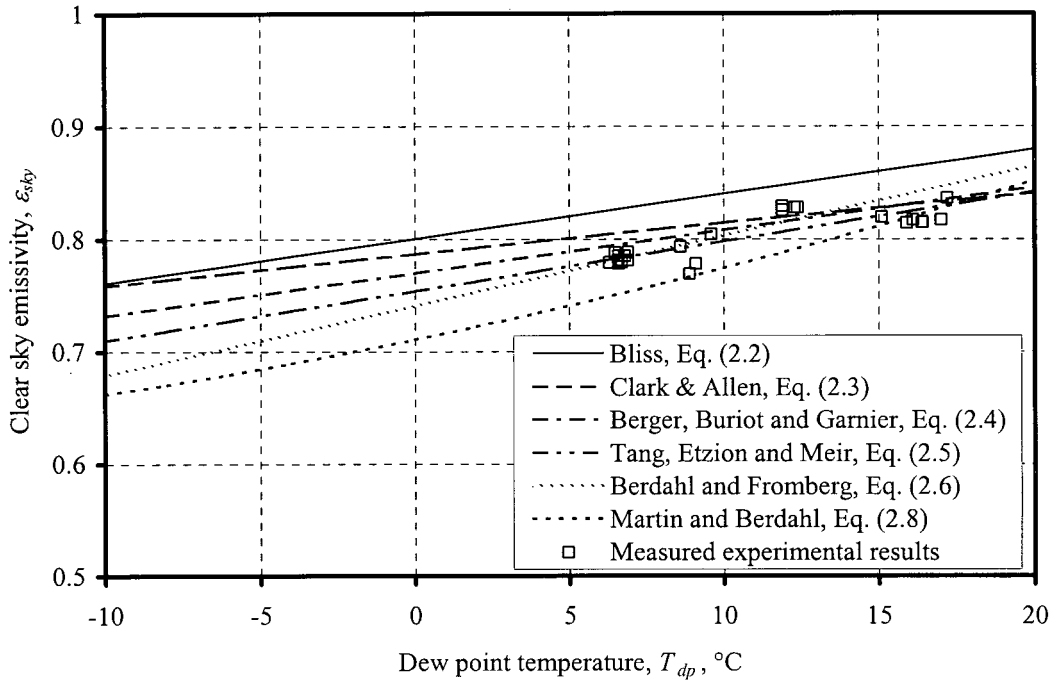

Figure 2.5: Nighttime clear sky emissivity at different dew point temperatures.

As can be seen in figures 2.4 and 2.5, the experimental results for the nighttime clear sky emissivity ε_{sky} are very well correlated by equation (2.6) given by Berdahl and Fromberg (1982) and equation (2.5) given by Tang, Etzion and Meir (2004).

As the equation by Tang, Etzion and Meir (2004) is only for nighttime clear sky emissivity the assumption was made that the equation by Berdahl and Fromberg (1982) for daytime clear sky emissivity is as accurate as the equation for the nighttime clear sky emissivity. It was thus decided to use the equations by Berdahl and Fromberg (1982) for the clear sky emissivity during day- or nighttime.

A sample calculation for calculating the clear sky emissivity is shown in Appendix A.

2.5 Conclusion

The nighttime clear sky emissivity has been studied experimentally. Equation (2.6) by Berdahl and Fromberg (1982) best correlates the experimental data. For the clear sky emissivity during daytime equation (2.7) by Berdahl and Fromberg (1982) will be used.

Chapter 3 Convection Heat Transfer Coefficient During Daytime

In this chapter the convection heat transfer coefficient between a large horizontal surface and the natural environment during daytime is determined experimentally. It is shown that for a surface that is warmer than the ambient air the heat is transferred due to natural and forced convection. The results are compared to values by other investigators. A good correlation is obtained between a new semi-empirical equation and the experimental results.

3.1 Introduction and Literature Review

Consider the energy balance that is applicable to a unit area of horizontal surface that is exposed to the natural environment on a clear, dry, sunny day, as shown in figure 3.1, i.e.

$$I_h\alpha_s = h(T_s - T_a) + (\varepsilon\sigma T_s^4 - \alpha_{lw}\sigma T_{sky}^4) - k_g(\mathrm{d}T/\mathrm{d}z) \tag{3.1}$$

where $I_h\alpha_s$ is the incident solar radiation absorbed per unit horizontal area.

Solar radiation is made up of two components, namely diffuse radiation I_d and beam radiation I_b, both of which are short wave radiation, i.e.

$$I_h = I_b + I_d \tag{3.2}$$

According to Duffie and Beckman (1991) the absorptivity α_z of most ordinary blackened surfaces is a function of incident angle, i.e.

$$\alpha_z = \alpha\left[1 + 2.0345\times10^{-3}\theta_z - 1.99\times10^{-4}\theta_z^{\,2} + 5.324\times10^{-6}\theta_z^{\,3} - 4.799\times10^{-8}\theta_z^{\,4}\right] \quad (3.3)$$

where α is the absorptivity of a surface at normal incidence and θ_z is the incidence angle in degrees.

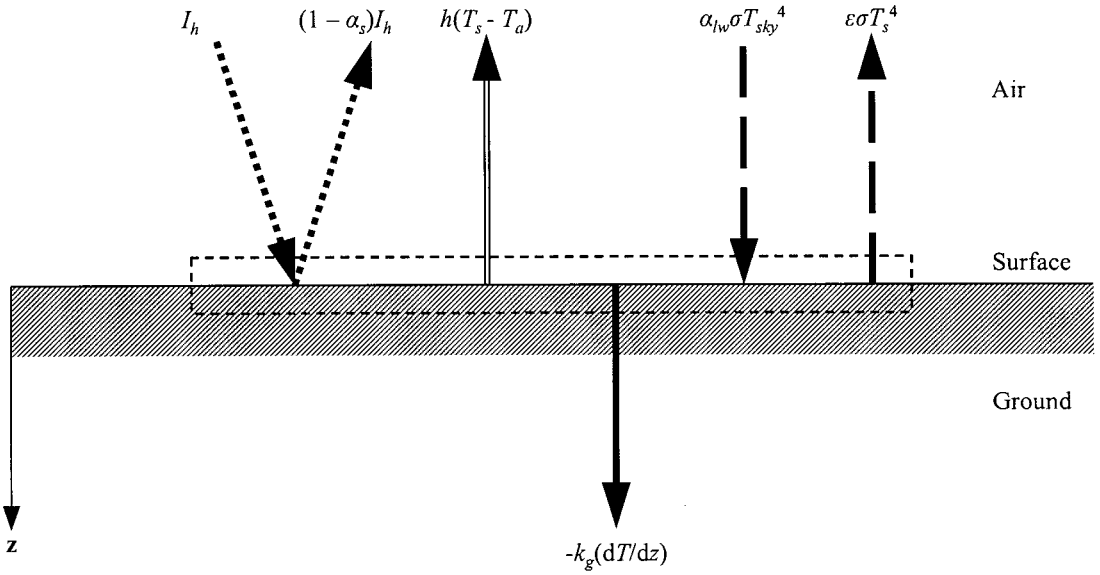

Figure 3.1: Heat fluxes at ground surface exposed to the environment during daytime.

For diffuse solar radiation I_d on a horizontal surface, the effective incidence angle θ_e is 60 °, while for beam radiation I_b on a horizontal surface, the incidence angle is equal to the zenith angle θ_z. The solar incident radiation absorbed by the horizontal surface is thus

$$\begin{aligned} I_h\alpha_s &= I_b\alpha_z + I_d\alpha_d \\ &= I_b\alpha\left[1 + 2.0345\times10^{-3}\theta_z - 1.99\times10^{-4}\theta_z^2 + 5.324\times10^{-6}\theta_z^3 - 4.799\times10^{-8}\theta_z^4\right] \\ &\quad + 0.9337 I_d\alpha \end{aligned} \quad (3.4)$$

The first term on the right-hand side of equation (3.1) represents the convective heat transfer between the surface and the ambient air. The objective of this chapter is to determine the heat transfer coefficient h.

The second term on the right-hand side of equation (3.1) represents the net long wave radiation between the surface and the environment. In this term, the Kelvin sky temperature is given by rearranging equation (2.1), i.e.

$$T_{sky} = [\varepsilon_{sky} T_a^4]^{1/4} \tag{3.5}$$

It was decided in chapter 2 to use the equation of Berdahl and Fromberg (1982) for clear sky emissivity. Berdahl and Fromberg (1982) recommend the following equation for clear sky emissivity during daytime:

$$\varepsilon_{sky} = 0.727 + 0.0060 T_{dp} \tag{2.7}$$

The third term on the right-hand side of equation (3.1) represents the heat conducted by the ground. If the surface is insulated, this term is negligible and the convection heat transfer coefficient is obtained by rearranging equation (3.1), i.e.

$$h = \frac{I_b \alpha_z + I_d \alpha_d - \left(\varepsilon \sigma T_s^{\ 4} - \alpha_{lw} \sigma T_{sky}^{\ 4}\right)}{T_s - T_a} \tag{3.6}$$

where $\alpha_z = \alpha[1 + 2.0345\times10^{-3}\theta_z - 1.99\times10^{-4}\theta_z^2 + 5.324\times10^{-6}\theta_z^3 - 4.799\times10^{-8}\theta_z^4]$

$\alpha_d = 0.9337\alpha$

The results of tests that were conducted on surfaces exposed to the natural environment during windy conditions are reported by Duffie and Beckmann (1991), Watmuff, Charters and Proctor (1977) and Test, Lessman and Johary (1981). The experiments done by Test, Lessman and Johary (1981) are for surfaces with a 40 ° inclination. In general the convection heat transfer coefficients for the tests mentioned above are expressed as

$$h = a + b v_w \tag{3.7}$$

where a and b are supposed to be constants and v_w is the wind speed. Examples of these correlations are shown in figure 3.2.

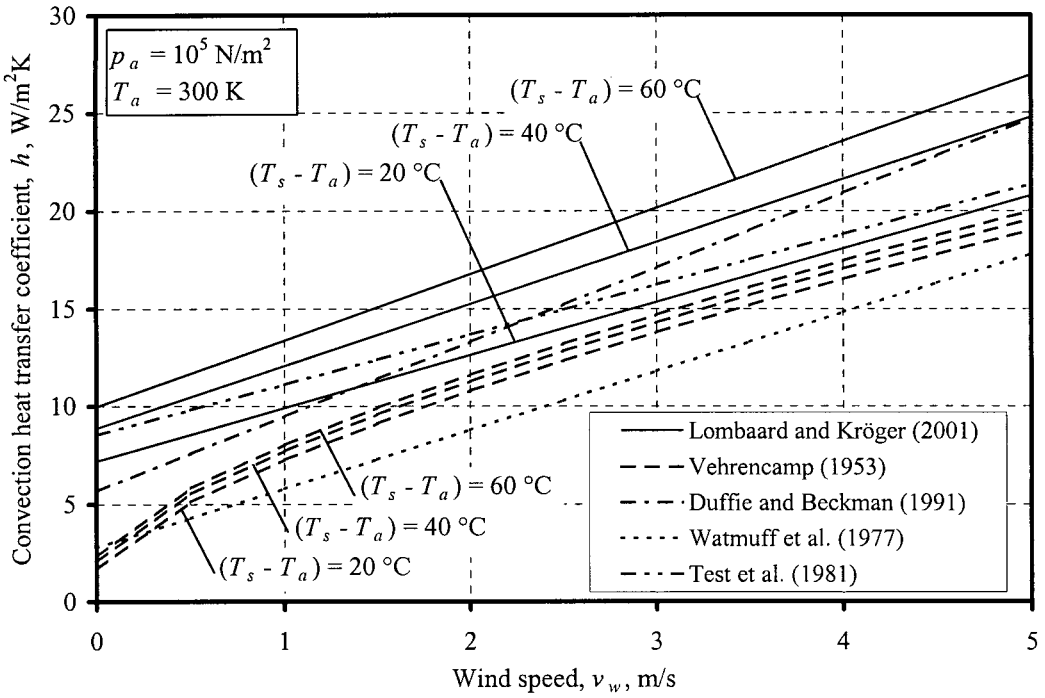

Figure 3.2: Heat transfer coefficient at different wind speeds.

A correlation by Vehrencamp (1953) that differs from equation (3.7) as well as a dimensionless equation according to Lombaard and Kröger (2001) is also shown. The equation given by Vehrencamp (1953) is used by Solaimanian and Kennedy (1993) and Hermansson (2004) for calculating the surface temperature of pavements. Note the significant discrepancies between the equations.

It is obvious that equation (3.7) cannot adequately express the convection heat transfer coefficient. Equation (3.7) is not dimensionless and does thus not make provision for changes in thermophysical properties. Furthermore, when the wind speed $v_w = 0$, heat that is transferred due to natural convection is not constant, but is a function of the temperature difference between the surface and the ambient air as given by Bejan (1984), i.e.

$$Nu = cRa^n \qquad n = 1/4 \text{ for } 10^4 \leq Ra \leq 10^7$$
$$n = 1/3 \text{ for } 10^7 \leq Ra \leq 10^{11}$$

For turbulent natural convection the equation can also be given by

$$h = c\left[\frac{g(T_s - T_a)c_p k^2 \rho^2}{\mu T_m}\right]^{1/3} \tag{3.8}$$

where c is a constant and $T_m = (T_s + T_a)/2$ is the mean temperature.

Many laboratory experiments have been conducted to determine the heat transfer coefficient due to turbulent natural convection from a heated, horizontal, upward-facing surface (Fujii and Imura (1972), Rohsenow et al. (1998), Lloyd and Moran (1974), Al-Arabi and El-Riedy (1976), Clausing and Berton (1989)). Values of c range between 0.13 and 0.16. In part, this range of values for c is due to the fact that the test surfaces were made up of different materials and had different sizes. In some tests uniform surface temperatures were maintained while in other cases it was assumed that the heat flux was uniform.

Lombaard and Kröger (2001) conducted experiments on an insulated 1 m × 1 m horizontal plate exposed to the natural environment. This truly uniform "heat flux" (solar radiation) test gave a value of $c = 0.227$.

Al-Arabi and El-Riedy (1976) refer to the work of Kraus who tested 160 mm × 160 mm to 260 mm × 260 mm heated horizontal surfaces and obtained a coefficient of $c = 0.137$ and Kamal and Salah who studied a horizontal rectangular plate 504 mm × 200 mm maintained at constant temperature and concluded that for a plate of infinite size (for which case the edge effects could be neglected) the value of the coefficient was $c = 0.135$. Al-Arabi and El-Riedy (1976) carried out experiments on upward facing heated plates at constant temperature. They tested square plates having dimensions varying from 50 mm to 450 mm, circular plates ranging from 100 mm to 500 mm in diameter and rectangular plates with a width of 150 mm and lengths of 250 mm to 600 mm. All their mean results are well correlated by a coefficient of $c = 0.155$. They also conducted an experiment on a square plate to find the heat transfer coefficient in the central part of the plate, which was not influenced by edge effects. The resultant coefficient had a value of $c = 0.145$.

According to the studies by Al-Arabi and El-Riedy (1976), it would thus appear that for an infinite horizontal surface at constant temperature, $c = 0.14$ (average of 0.135 and 0.145).

According to Kröger (2002) the value of the constant for uniform surface heat flux is $\pi/2$ times this value, i.e. 0.22. This value is close to the 0.227 found by Lombaard and Kröger (2001).

Kröger (2002) theoretically analysed the problem of convection heat transfer on a horizontal surface exposed to the natural environment. He shows that the dimensionless convective heat transfer coefficient is given by

$$h\left[\frac{\mu T_m}{g(T_s-T_a)c_p k^2 \rho^2}\right]^{1/3} = c + v_w\left(\frac{C_f}{2}\right)\left[\frac{\rho T_m}{\mu g(T_s-T_a)}\right]^{1/3} \tag{3.9}$$

In this approximate, semi-empirical equation the constant c has a theoretical value of 0.243. The effective friction coefficient, C_f, has to be determined experimentally under windy conditions.

3.2 Experimental Set-up and Procedures

Experiments were conducted at the Solar Energy Laboratory of the University of Stellenbosch, Stellenbosch, South Africa (Altitude 100 m, Latitude –33.93 °, Longitude 341.15 ° west). The experimental apparatus consisted of a 1 m × 1 m polystyrene plate having a thickness of 50 mm, which was surrounded by an open area covered with a large black plastic sheet as shown schematically in figure 3.3.

The plate was painted matt black and was put on the black sheet to simulate an infinite black surface and to minimise edge effects. The solar absorptivity α_s of the black painted surface is 0.93, while the long wave emissivity ε and absorptivity α_{lw} is 0.90.

The surface temperature measurements were obtained from six type T thermocouples that were embedded on the surface of the plate. Another four type T thermocouples were placed at different heights above the solar collector, as shown in figure 3.3, to measure the temperature gradient above the collector.

A weather station was used to measure ambient air temperature, dew point temperature, barometric pressure, humidity, wind speed and wind direction 1 m above the surface of the polystyrene plate. The wind speed was also measured at 0.15 m above ground level. Solar radiation was measured with a Kipp & Zonen pyranometer. All data was collected in one minute intervals and averaged over ten minutes.

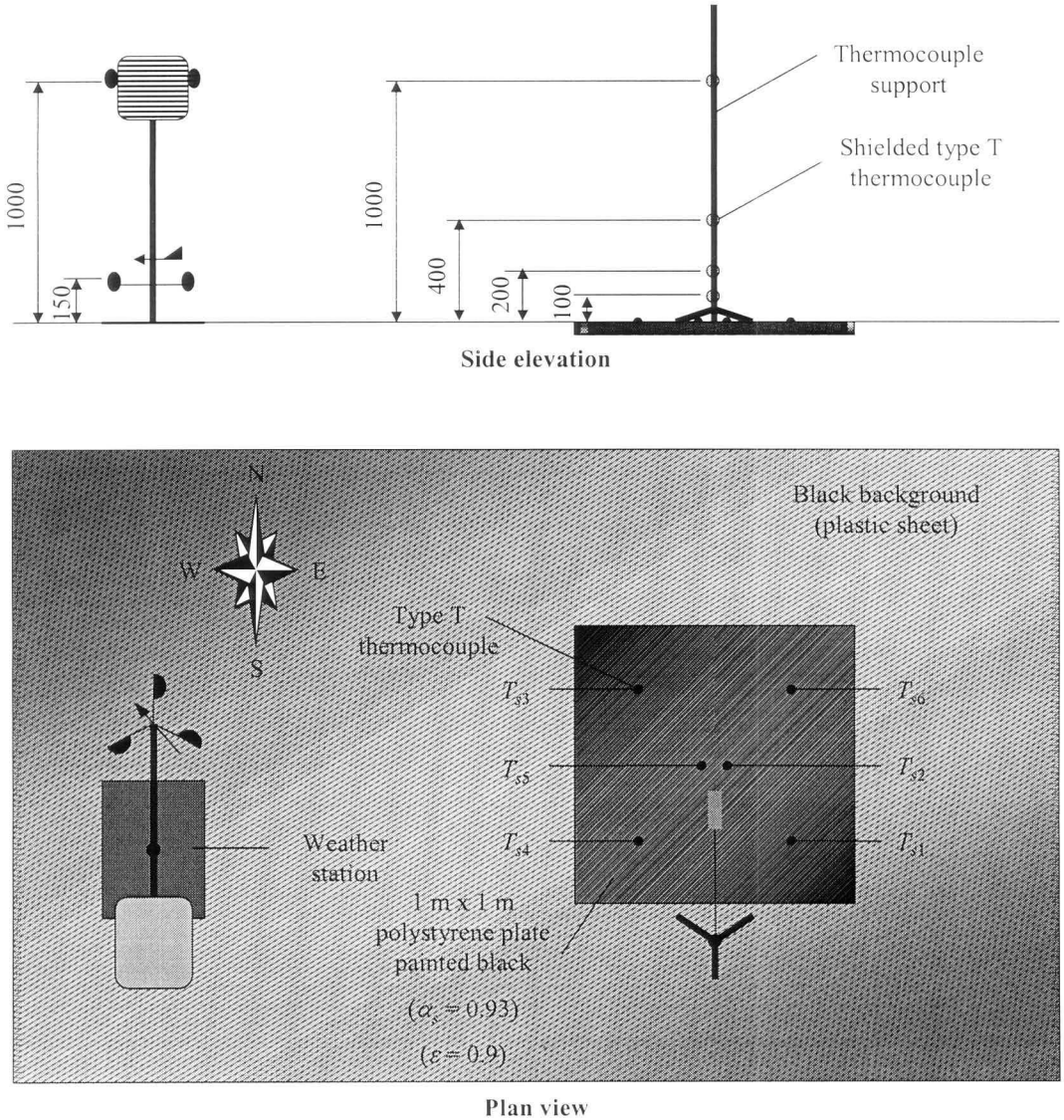

Figure 3.3: Schematic of the experimental set-up.

The zenith angle was determined by measuring the horizontal length of the shadow of a vertical pole with a known length and then calculating the angle between the vertical pole and the angle of incidence of the beam radiation. Examples of experimental measurements as a function of solar time on a particular day are shown graphically in figures 3.4 to 3.7.

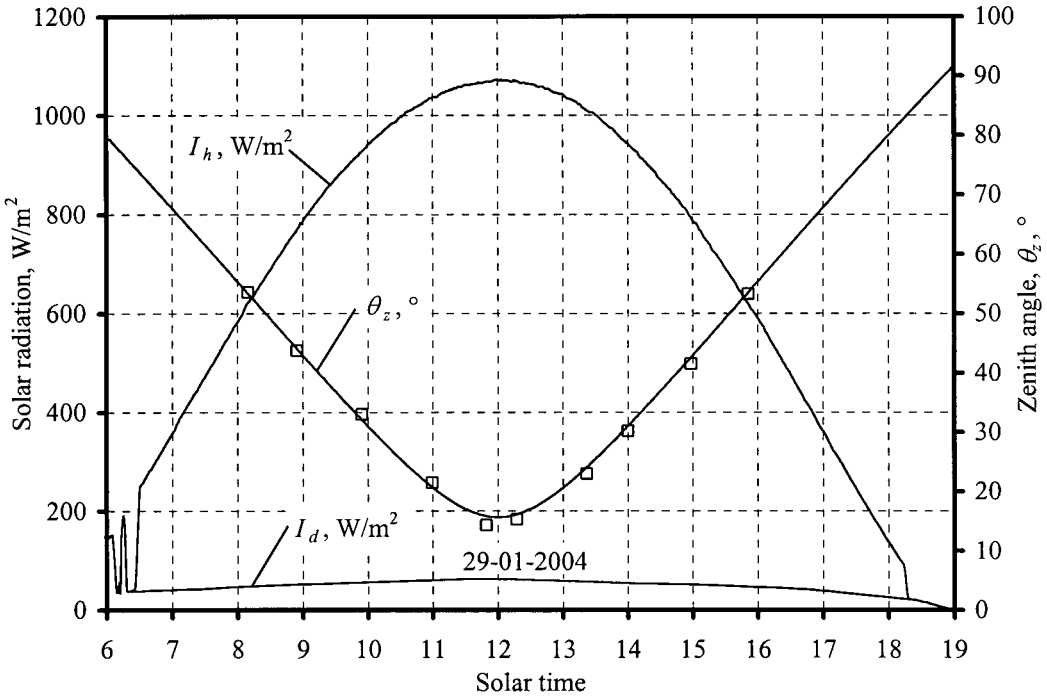

Figure 3.4: Measured solar radiation and zenith angle.

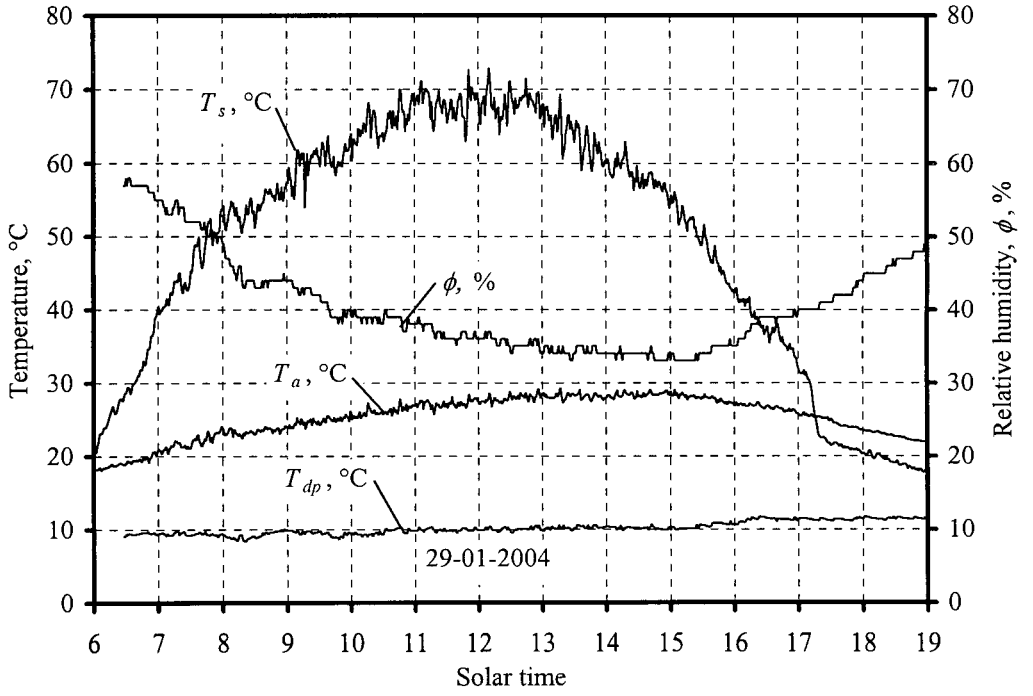

Figure 3.5: Measured surface, ambient air and dew point temperature and relative humidity.

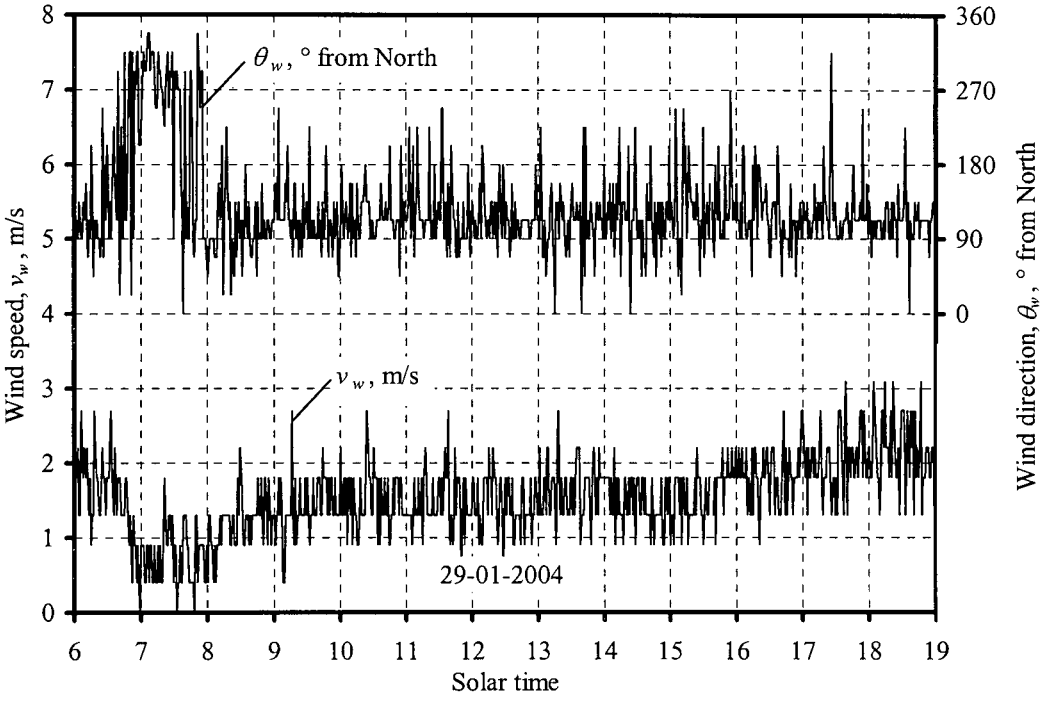

Figure 3.6: Measured wind speed and direction at a height of 0.15 m above ground level.

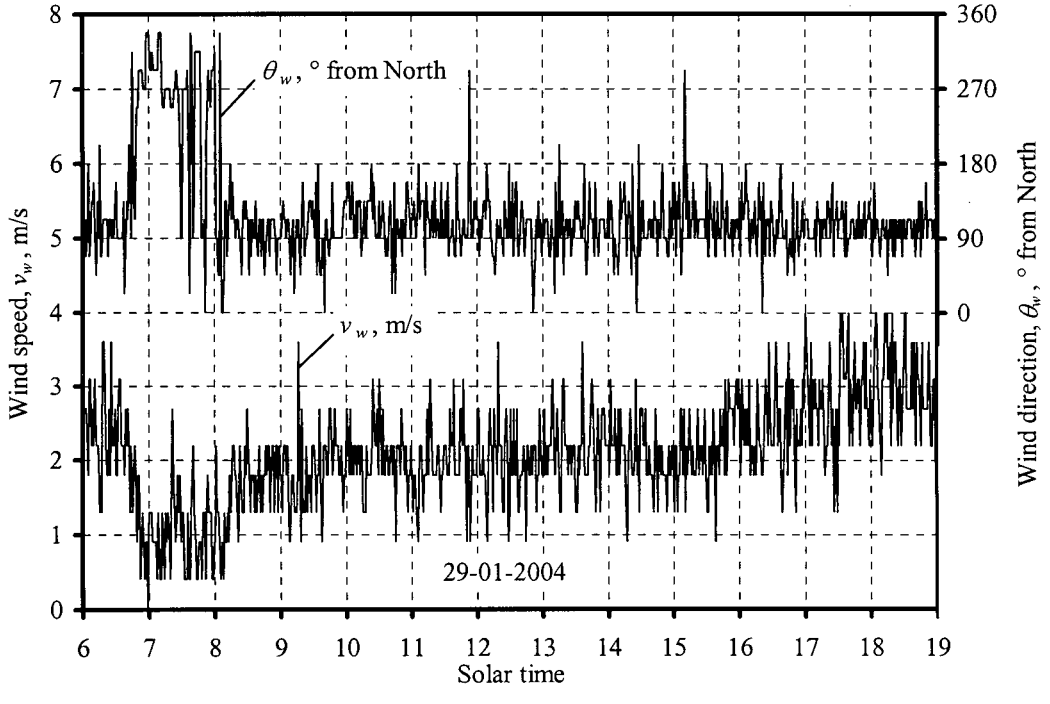

Figure 3.7: Measured wind speed and direction at a height of 1 m above ground level.

3.3 Results and Discussion

As shown in figure 3.8 the experimental results for the dimensional heat transfer coefficient are well correlated by an expression having the same form as equation (3.9), i.e.

$$h\left[\frac{\mu T_m}{g(T_s-T_a)c_p k^2\rho^2}\right]^{1/3} = 0.2106 + 0.0026 v_w \left[\frac{\rho T_m}{\mu g(T_s-T_a)}\right]^{1/3} \qquad (3.10)$$

in the range of $0 \le v_w\left[\frac{\rho T_m}{\mu g(T_s-T_a)}\right]^{1/3} \le 160$ and $0\,\text{m/s} \le v_w \le 4\,\text{m/s}$.

The value of the coefficient c of 0.2106 is close to the expected value of $0.14(\pi/2) = 0.22$. The value of the effective friction coefficient based on a height of 1.0 m above ground level is $C_f = 0.0052$.

Figure 3.9 shows the left-hand side of equation (3.9) and the long wave sky radiation as a function of solar time.

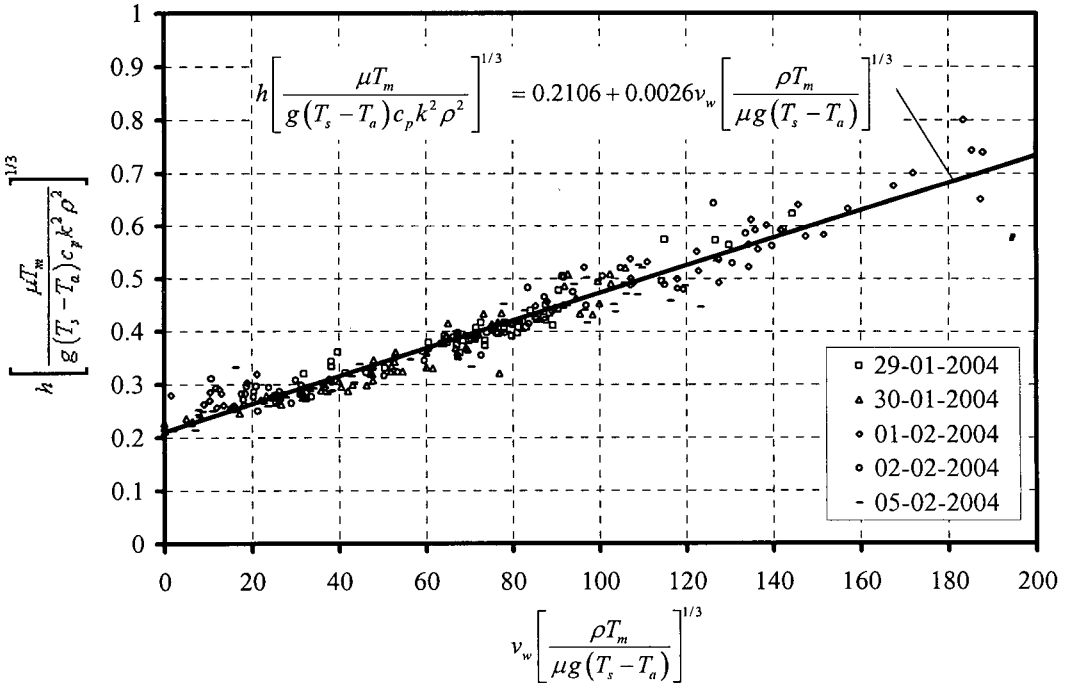

Figure 3.8: Experimental results of the dimensional heat transfer coefficient.

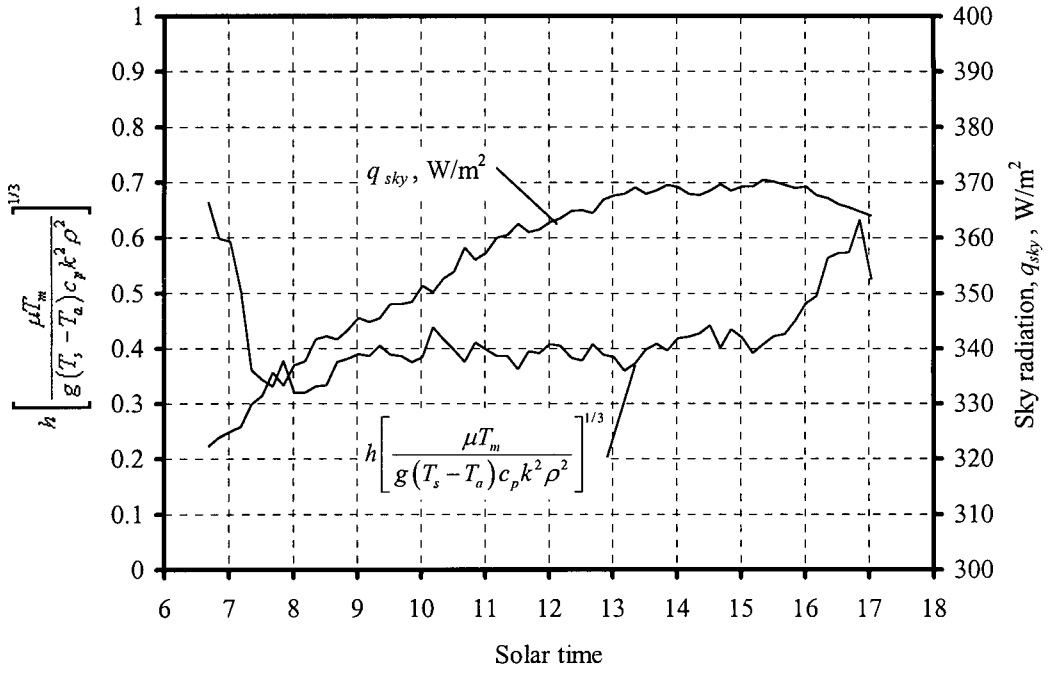

Figure 3.9: Left-hand side of equation (3.9) and the long wave sky radiation as a function of solar time.

A sample of the calculation of the convection heat transfer coefficient is given in Appendix B.

3.4 Conclusion

The convection heat transfer coefficient between an infinite horizontal surface and the natural environment during daytime has been determined experimentally. The experimental data is well correlated by equation (3.10) in the range of 0 m/s $\leq v_w \leq$ 4 m/s, measured 1 m above ground level. The value of the effective skin friction coefficient, based on a height of 1 m above ground level, is found to be $C_f = 0.0052$.

Chapter 4 Convection Heat Transfer Coefficient During Nighttime

In the following chapter the convection heat transfer coefficient between an infinite horizontal surface and the natural environment during nighttime is determined experimentally. It is shown that during periods of no wind heat is transferred due to a mixture of convection and conduction, while during windy periods heat is transferred due to forced convection. A good correlation is obtained between a semi-empirical equation and the experimental data.

4.1 Introduction and Literature Review

Considering figure 2.1 for a horizontal surface exposed to the natural environment during the night. The second term on the right-hand side of equation (2.12) can be neglected for an insulated surface to give

$$h\,(T_a - T_s) = (\varepsilon\sigma T_s^{\,4} - \alpha_{lw}\sigma T_{sky}^{\,4}) \tag{4.1}$$

or

$$h = \frac{\left(\varepsilon\sigma T_s^{\,4} - \alpha_{lw}\sigma T_{sky}^{\,4}\right)}{\left(T_a - T_s\right)} \tag{4.2}$$

where T_{sky} is given by equation (3.5) with the use of equation (2.6) for the calculation of the clear sky emissivity during nighttime.

During windy periods the Reynolds-Colburn analogy, as reported by Kröger (2002), and used in chapter 3 for the determination of the forced convection heat transfer coefficient is used, i.e.

$$h_{fc} = \frac{C_f \rho c_p v_w}{2\left(\mu c_p / k\right)^{2/3}} \tag{4.3}$$

where the skin friction coefficient C_f has to be determined experimentally.

Published correlations (Mills (1995)) for the heat transfer coefficient in the absence of wind on finite, cooled, surfaces facing upwards are of the form

$$\overline{Nu_L} = \frac{\bar{h}L}{k} = cRa_L^{1/5} \tag{4.4}$$

where $\overline{Nu_L}$ is the averaged Nusselt number, c is a constant, Ra_L is the Rayleigh number and L is the side length of a square plate or the length of the shorter side of a rectangular plate. There is however no correlation for an infinite surface.

In the case of an infinite, horizontal, cooled surface the transfer of heat is essentially due to conduction.

4.2 Experimental Set-up and Procedures

The same experimental set-up and procedures were used in determining the effective convection heat transfer coefficient during nighttime as during daytime experiments (chapter 3). Examples of experimental measurements as a function of solar time on a particular day are shown graphically in figures 4.1 to 4.3.

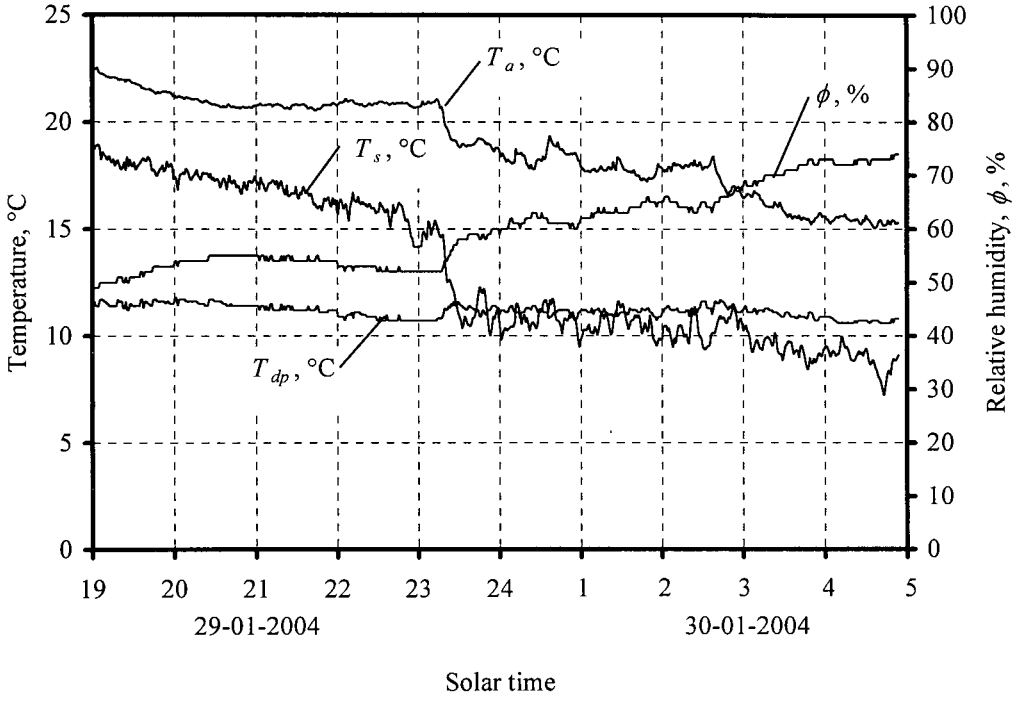

Figure 4.1: Measured surface, ambient air and dew point temperature and relative humidity.

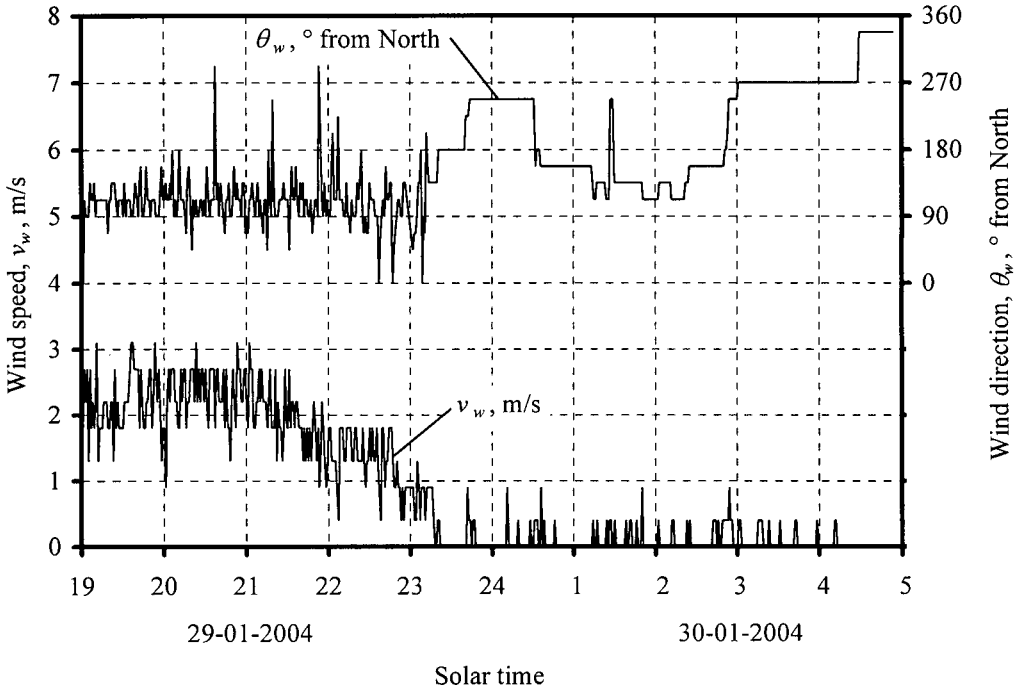

Figure 4.2: Measured wind speed and direction at a height of 0.15 m above ground level.

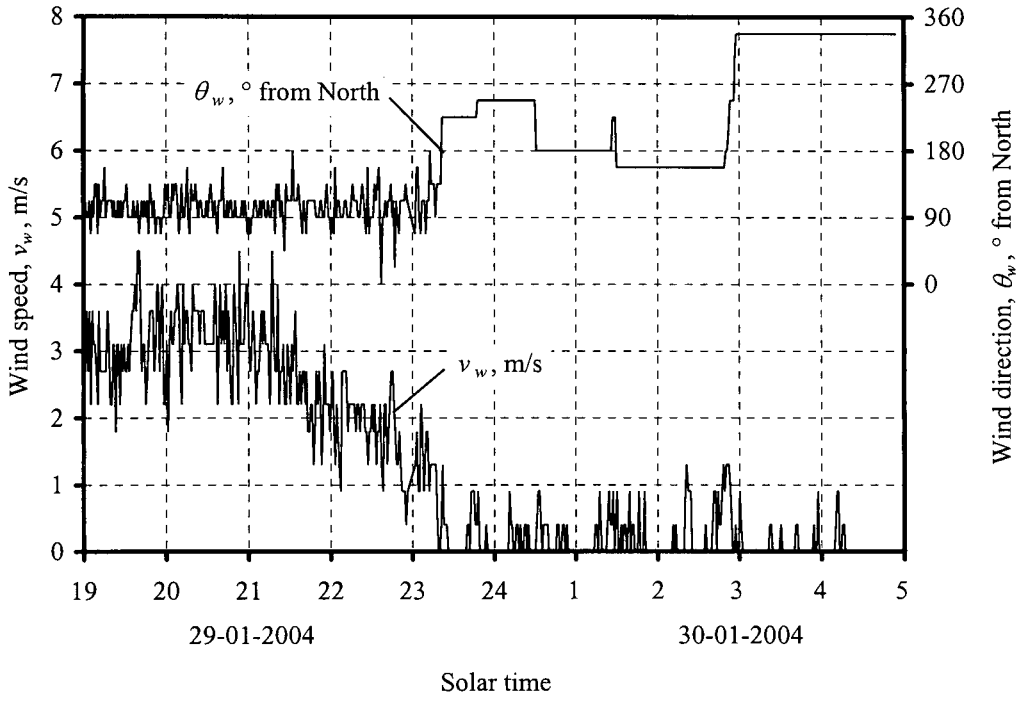

Figure 4.3: Measured wind speed and direction at a height of 1 m above ground level.

4.3 Results and Discussion

As shown in figure 4.4 the experimental results for the heat transfer coefficient are well correlated by an expression having the same form as equation (4.3), but with an additional effective heat transfer coefficient at a wind speed v_w of 0 m/s, i.e.

$$h = 3.87 + 0.0022 \frac{v_w \rho c_p}{\left(\mu c_p / k\right)^{2/3}} \tag{4.5}$$

in the range of $0 \leq \frac{v_w \rho c_p}{\left(\mu c_p / k\right)^{2/3}} \leq 160$ and $0\,\text{m/s} \leq v_w \leq 5\,\text{m/s}$.

From figure 4.1 can be seen that during times of low or no wind speed the surface temperature T_s is equal or lower than the dew point temperature T_{dp}. Even with the weather station measuring no wind there is still movement in the air so the constant heat transfer coefficient of 3.87 at no wind is a mixed conduction, convection and condensation heat transfer term.

Figure 4.5 shows the convection heat transfer coefficient and the long wave sky radiation as a function of solar time for a particular night.

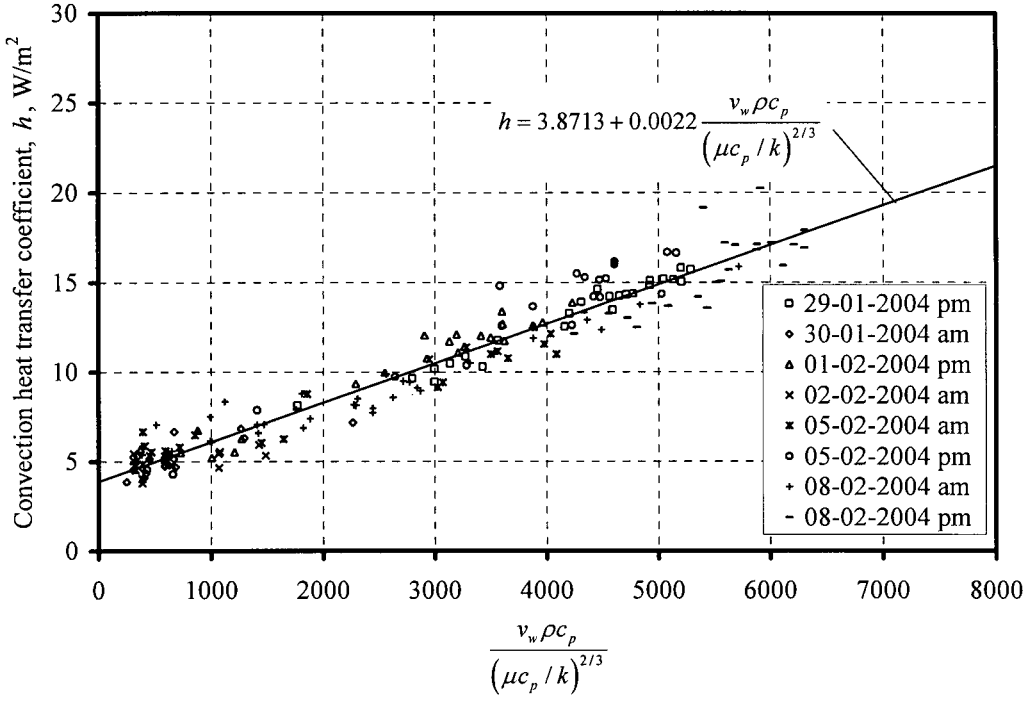

Figure 4.4: Experimental results of the convection heat transfer coefficient.

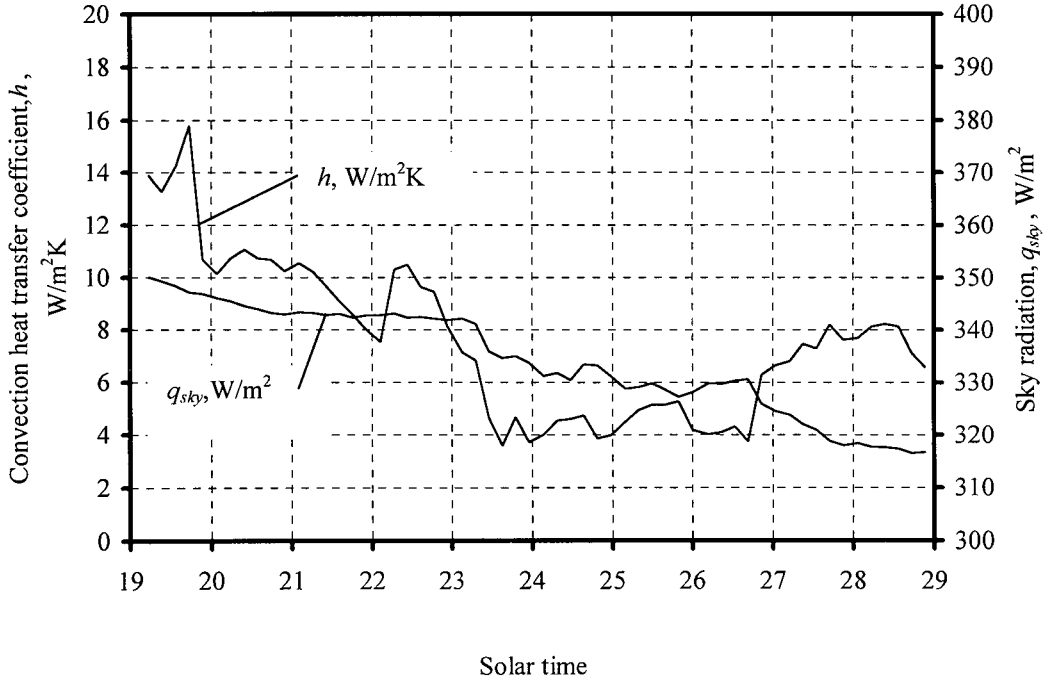

Figure 4.5: Convection heat transfer coefficient and the long wave sky radiation.

The value of the effective friction coefficient based on a height of 1 m above ground level is $C_f = 0.0044$.

A sample of the calculation of the heat transfer coefficient is given in Appendix C.

4.4 Conclusion

The effective convection heat transfer coefficient between an infinite horizontal surface and the natural environment during nighttime has been determined experimentally. The experimental data is well correlated by equation (4.5) in the range of 0 m/s $\leq v_w \leq$ 5 m/s, measured 1 m above ground level. The value of the effective skin friction coefficient, based on a height of 1 m above ground level, is found to be $C_f = 0.0044$.

Chapter 5 Predicting the Pavement Temperature Distribution

In this chapter the measured surface temperature and the temperature at depth of asphalt pavement samples is compared with the calculated temperatures using a simulation model. The input data for the model is ambient air temperature, solar radiation, dew point temperature, wind speed and barometric pressure at one-minute intervals.

5.1 Introduction and Literature Review

Predicting the temperature at any depth in an asphalt pavement is important for designing and choosing the right binder and mixture specification. During summer the high solar radiation and air temperatures can cause the pavement to become soft and heavy vehicles can cause rutting due to plastic deformation.

In the literature there are a few empirical equations with which the pavement surface temperature and temperatures at depth can be calculated. As reported by Everitt et. al. (1999) the Strategic Highway Research Program (SHRP) has developed a model (Superpave) that makes use of environmental data to characterise the required binder properties of expected pavement temperatures. They use a rigorous equation, which has to be solved with numerical analysis, to calculate the maximum pavement surface temperature, i.e.

$$1331\alpha\tau_a^{1/\cos\Phi}\cos\Phi + \varepsilon_{sky}\sigma T_a^4 - h(T_s - T_a) - 164k - \varepsilon\sigma T_s^4 = 0 \qquad (5.1)$$

where α is the pavement surface solar absorptivity, τ_a is the air transmission coefficient, Φ is the location latitude, ε_{sky} is the air emissivity, T_a is the ambient air temperature in K, h is the convection heat transfer coefficient, T_s is the pavement surface temperature in K and k is the thermal conductivity of the pavement.

To simplify calculations the Superpave procedures recommend that pavement surface temperature be calculated using the following empirical, regression equation proposed by Huber (1994).

$$T_s = T_a - 0.00618\Phi^2 + 0.2289\Phi + 24.4 \tag{5.2}$$

Superpave also recommends the following equation to convert surface temperature to pavement temperature at depth.

$$T_d = (T_s + 17.8)(1 - 2.48 \times 10^{-3}d + 1.085 \times 10^{-5}d^2 - 2.441 \times 10^{-8}d^3) - 17.8 \tag{5.3}$$

where T_d is the pavement temperature at depth d from the surface in °C.

Equations (5.2) and (5.3) cannot be accurate as they do not take into account any wind, solar radiation or pavement thermal properties.

Solaimanian and Kennedy (1993) use a method that is based on an energy balance at the pavement surface and has the same form as equation (5.1), i.e.

$$1394\alpha\tau_a^{1/\cos\Phi}\cos\Phi + \varepsilon_{sky}\sigma T_a^4 - h(T_s - T_a) - k(T_s - T_d)/d - \varepsilon\sigma T_s^4 = 0 \tag{5.4}$$

The first term of equation (5.4) represents the absorbed solar radiation, the second term represents the absorbed long wave radiation from the sky, the third term is the convection heat transfer between the surface and the ambient air, the fourth term is the heat conduction in the pavement and the fifth term represents the long wave radiation radiated by the surface.

5.2 Analysis

5.2.1 Pavement Surface

Consider the control volume that is applicable to a unit area of pavement surface that is exposed to the natural environment as shown in figure 5.1, i.e.

$$I_h\alpha_s = h(T_s - T_a) + (\varepsilon\sigma T_s^4 - \alpha_{lw}\sigma T_{sky}^4) - k_g(\mathrm{d}T/\mathrm{d}z) \tag{5.5}$$

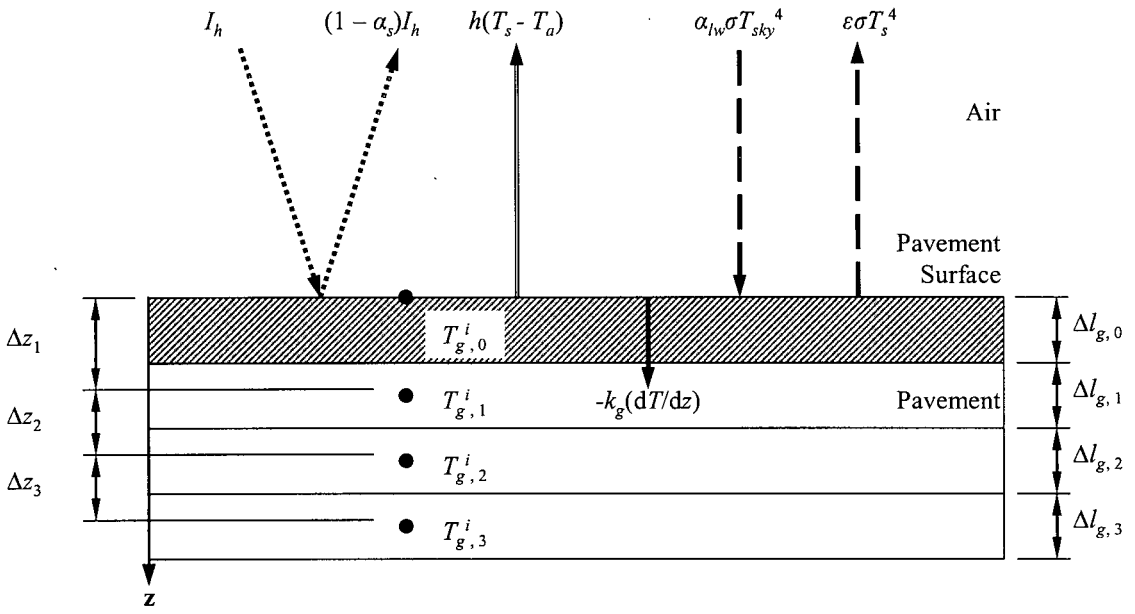

Figure 5.1: Control volume of a unit area of pavement surface exposed to the natural environment.

If one assumes one-dimensional unsteady conduction in the pavement over a time interval dt, equation (5.5) changes to

$$I_h\alpha_s = h(T_s - T_a) + (\varepsilon\sigma T_s^4 - \alpha_{lw}\sigma T_{sky}^4) - k_g(\mathrm{d}T/\mathrm{d}z) + \rho_g\Delta l_g c_{pg}(\mathrm{d}T/\mathrm{d}t) \tag{5.6}$$

The fourth term on the right-hand side of equation (5.6) is the increase in internal energy of the control volume over a time step dt, from time step i to step $(i + 1)$. Discretizing equation (5.6) gives

$$I_h\alpha_s = h\left(T_{g,0}^{i+1} - T_a\right) + \left(\varepsilon\sigma\left(T_{g,0}^{i+1}\right)^4 - \alpha_{lw}\sigma T_{sky}{}^4\right) - k_g \frac{T_{g,1}^{i} - T_{g,0}^{i+1}}{\Delta z_1} + \rho_g \Delta l_{g,0} c_{pg} \frac{T_{g,0}^{i+1} - T_{g,0}^{i}}{\Delta t} \tag{5.7}$$

where $T_{g,0}^{i+1}$ is the surface temperature of the pavement at time step $(i + 1)$.

During nighttime with no solar radiation, the term on the left-hand side of equation (5.7) is negligible and equation (5.7) changes to

$$0 = h\left(T_{g,0}^{i+1} - T_a\right) + \left(\varepsilon\sigma\left(T_{g,0}^{i+1}\right)^4 - \alpha_{lw}\sigma T_{sky}{}^4\right) - k_g \frac{T_{g,1}^{i} - T_{g,0}^{i+1}}{\Delta z_1} + \rho_g \Delta l_{g,0} c_{pg} \frac{T_{g,0}^{i+1} - T_{g,0}^{i}}{\Delta t} \tag{5.8}$$

For the convection heat transfer coefficient h during periods when the surface temperature is warmer than the ambient air temperature equation (3.10) is used and for periods when the surface temperature is colder than the ambient air temperature equation (4.5) is used.

5.2.2 Core of Pavement

Consider the control volume for a unit area layer of pavement underneath the surface as shown in figure 5.2.

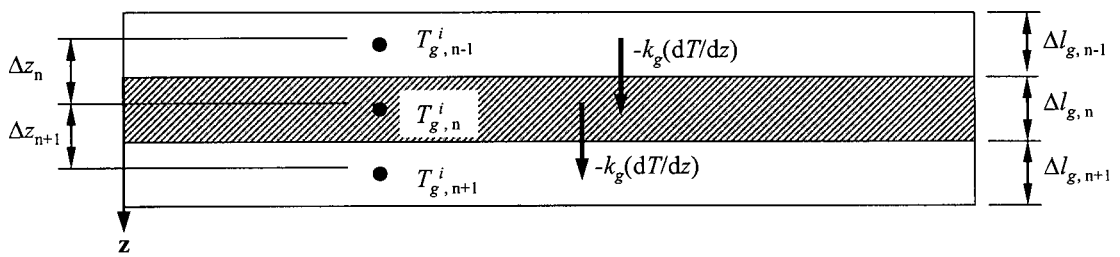

Figure 5.2: Control volume for a unit area layer of pavement underneath the surface.

Assuming one-dimensional unsteady conduction over a time interval dt, gives

$$-k_g(\mathrm{d}T/\mathrm{d}z)_{in} = -k_g(\mathrm{d}T/\mathrm{d}z)_{out} + \rho_g \Delta l_g c_{pg}(\mathrm{d}T/\mathrm{d}t) \tag{5.9}$$

Discretizing equation (5.9) gives

$$-k_g \frac{T_{g,n}^{i+1} - T_{g,n-1}^{i+1}}{\Delta z_n} = -k_g \frac{T_{g,n+1}^{i} - T_{g,n}^{i+1}}{\Delta z_{n+1}} + \rho_g \Delta l_{g,n} c_{pg} \frac{T_{g,n}^{i+1} - T_{g,n}^{i}}{\Delta t} \tag{5.10}$$

where $T_{g,n}^{i+1}$ is the temperature of the pavement at node n at time step $(i + 1)$.

5.2.3 Bottom of Pavement

From figure 5.3 the energy balance for the bottom layer of an insulated pavement, with unsteady one-dimensional conduction over a time interval dt, is given as

$$-k_g(\mathrm{d}T/\mathrm{d}z) = \rho_g \Delta t_g c_{pg}(\mathrm{d}T/\mathrm{d}t) \tag{5.11}$$

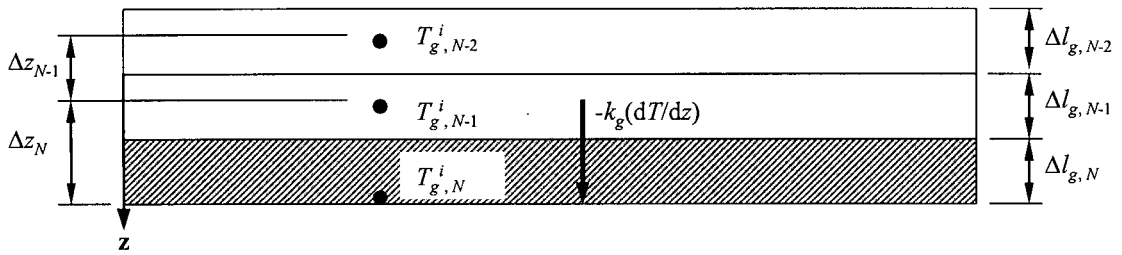

Figure 5.3: Control volume for a unit area bottom layer of an insulated pavement.

Discretizing equation (5.11) gives

$$-k_g \frac{T_{g,N}^{i+1} - T_{g,N-1}^{i+1}}{\Delta z_N} = \rho_g \Delta l_{g,N} c_{pg} \frac{T_{g,N}^{i+1} - T_{g,N}^{i}}{\Delta t} \tag{5.12}$$

where $T_{g,N}^{i+1}$ is the temperature of the bottom of the pavement sample at time step $(i + 1)$.

5.3 Experimental Set-up and Procedures

Figure 5.4 shows a schematic of the experimental set-up. It consisted of four asphalt pavement samples with two different aggregate gradations. Two of the samples were made from continuously graded wearing course mix (mix A) and the other two were an asphalt base mix with 26.5 mm maximum stone size (mix B). The samples had a diameter of 150 mm with the mix A samples having a thickness of 60 mm and the mix B samples a thickness of 50 mm. The samples were fitted in holes cut in a 1 m x 1 m piece of polystyrene.

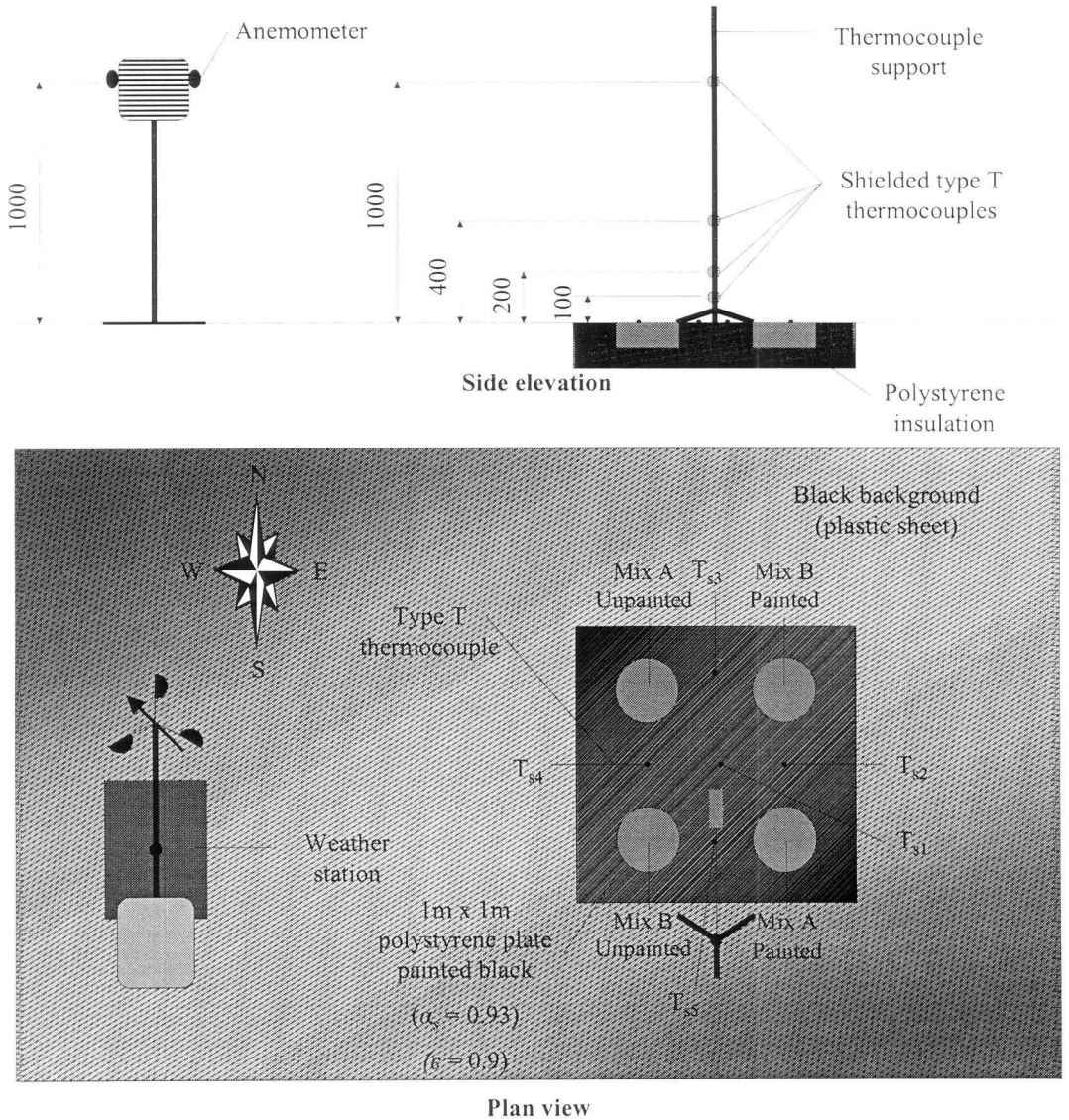

Figure 5.4: Schematic of the experimental set-up.

The upper surface temperatures of the pavement samples were measured with type T thermocouples imbedded in the asphalt at the surface. The temperature distribution in the samples were also measured, at different depths, with type T thermocouples, which were inserted through holes drilled from the side of the samples as shown in figure 5.5. The surface of one of the mix A samples and one of the mix B samples were painted black while the colour of other two samples' surfaces were kept natural. As mentioned in chaper 2 the solar absorptivity α_s of most black painted surfaces is 0.93, while the longwave emissivity ε and absorptivity α_{lw} is 0.90. The solar absorptivity of asphalt, according to Solaimanian and Kennedy (1993), has an average of about 0.9 and according to Mills (1995) the emissivity is 0.88. The surface of the polystyrene was also painted black with the same paint.

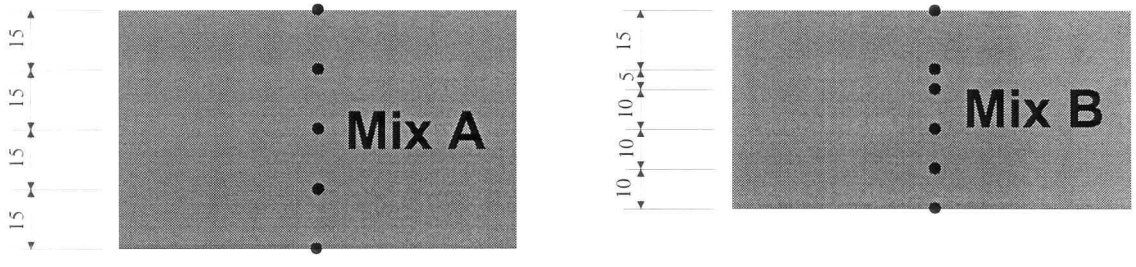

Figure 5.5: Thermocouple measuring depths.

The specific heat c_{pg} and diffusivity α_g of the pavement samples were determined experimentally and the results are shown in Appendix E. A thermal conductivity k_g of 1.4 W/mK for the mix A samples and 1.7 W/mK for the mix B samples was used to calculate the diffusivity. The experimental results gave a diffusivity α_g of 6.084×10^{-7} m/s^2 for the mix A samples and 8.072×10^{-7} m/s^2 for the mix B samples. These diffusivity values are close to the values determined by Highter and Wall (1984). For the best simulation results a thermal conductivity k_g of 1.4 W/mK and a diffusivity α_g of 6.94×10^{-7} m/s^2 was used for mix A, while for mix B a conductivity of 1.7 W/mK and a diffusivity of 8.94×10^{-7} m/s^2 was used.

The polystyrene surface temperature measurements were measured with five type T thermocouples that were embedded on the surface of the plate. Another four type T thermocouples were placed at different heights above the plate, as shown in figure 5.4, to

measure the temperature distribution above the plate.

A weather station was used to measure ambient air temperature, dew point temperature, barometric pressure, humidity, wind speed and wind direction at a height of 1 m above the surface. Solar radiation was measured with a Kipp & Zonen pyranometer.

All the data was measured in one-minute intervals. Examples of experimental measurements as a function of solar time of three consecutive days are shown graphically in figures 5.6 to 5.12.

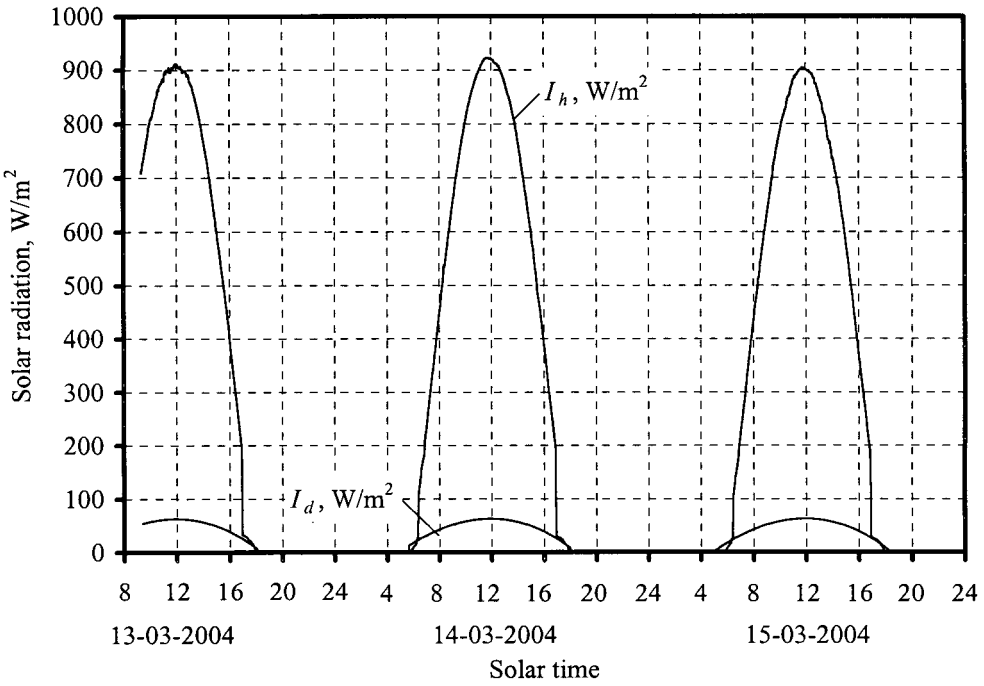

Figure 5.6: Measured solar radiation.

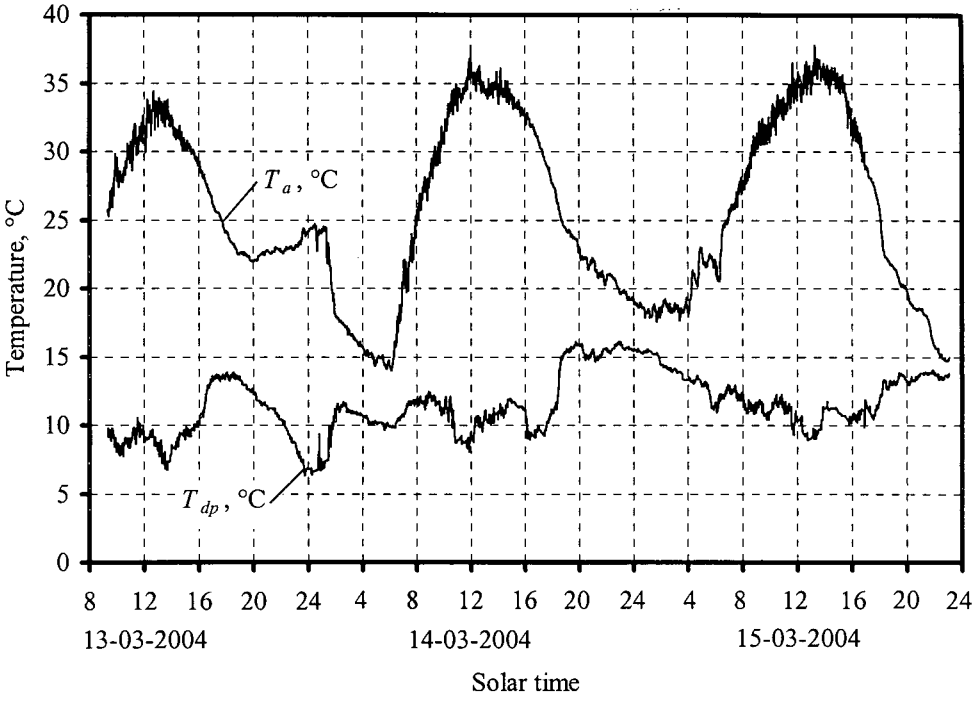

Figure 5.7: Measured ambient air temperature and dew point temperature.

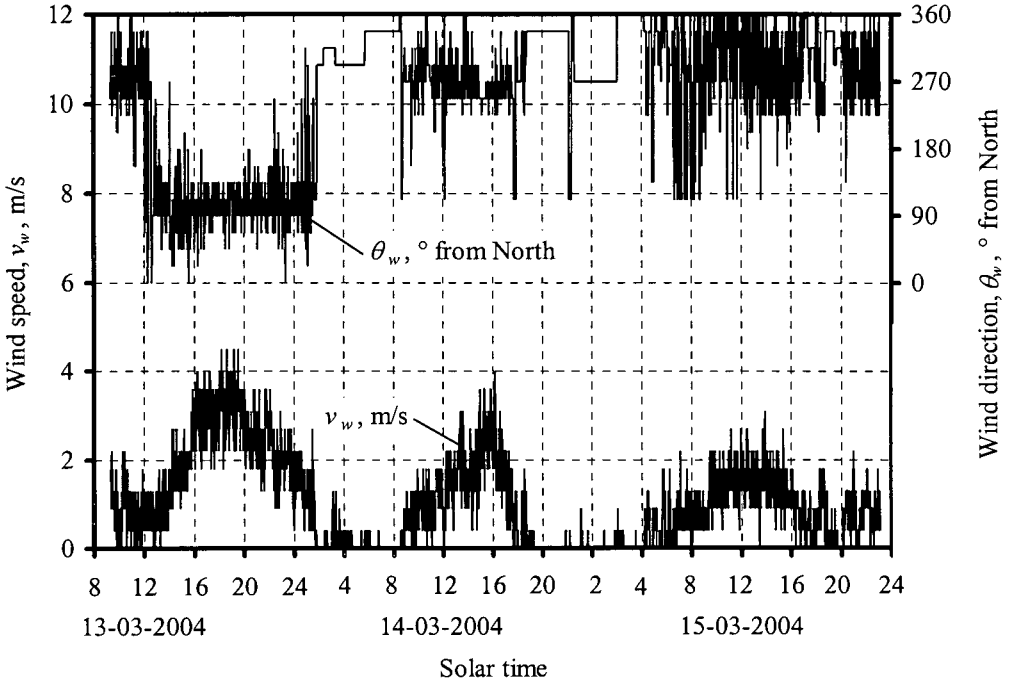

Figure 5.8: Measured wind speed and wind direction.

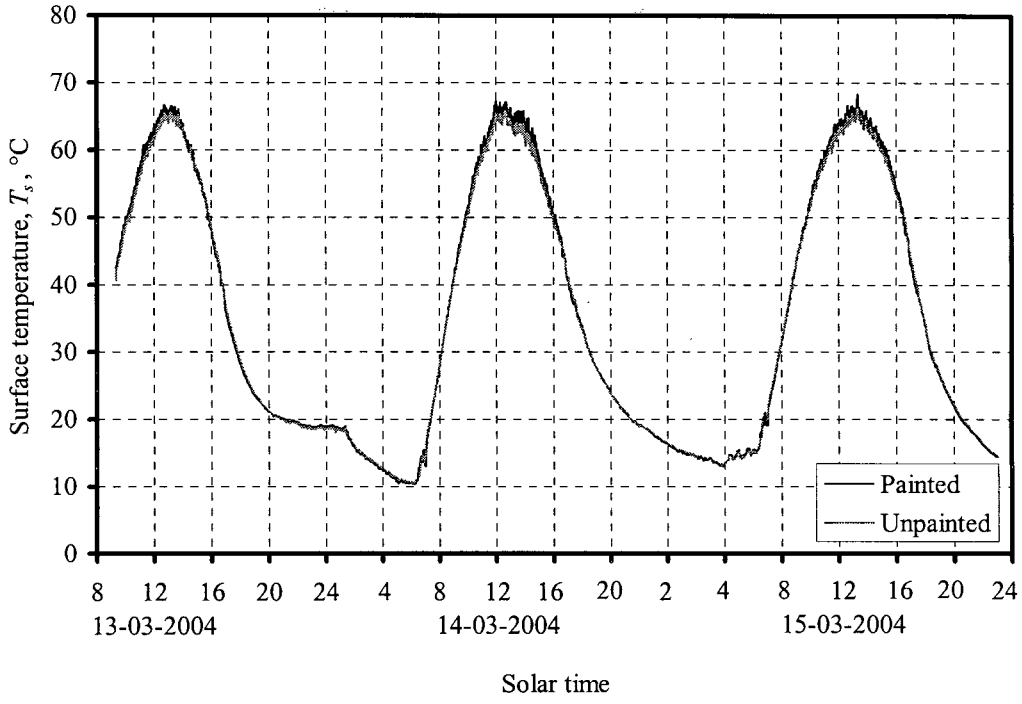

Figure 5.9: Measured surface temperatures of the two mix A samples.

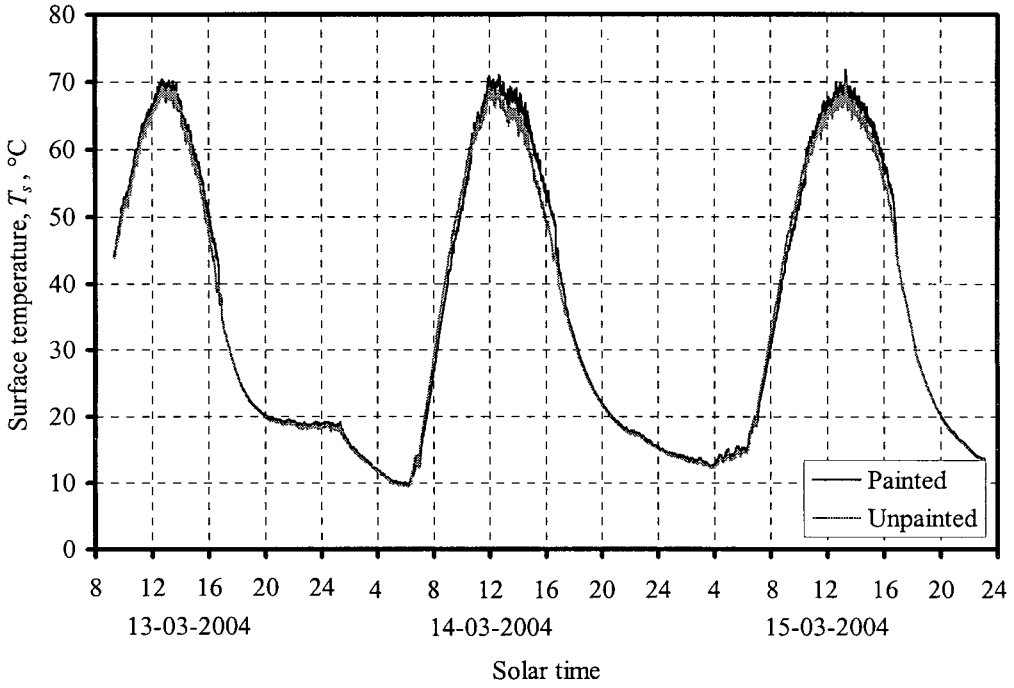

Figure 5.10: Measured surface temperatures of the two mix B samples.

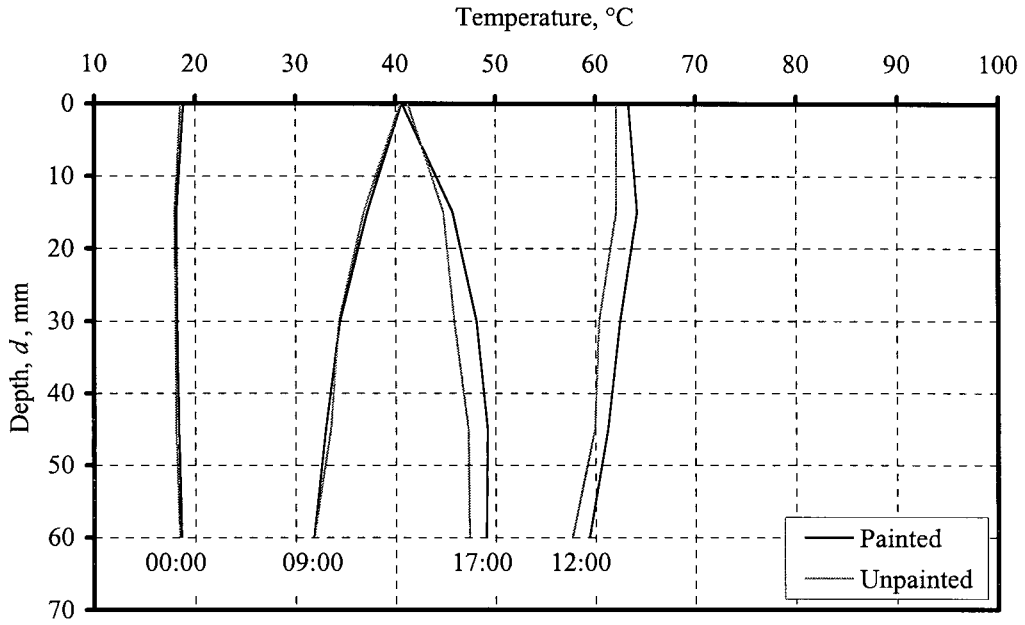

Figure 5.11: Temperature distribution at certain times on 14-03-2004 in the two mix A samples.

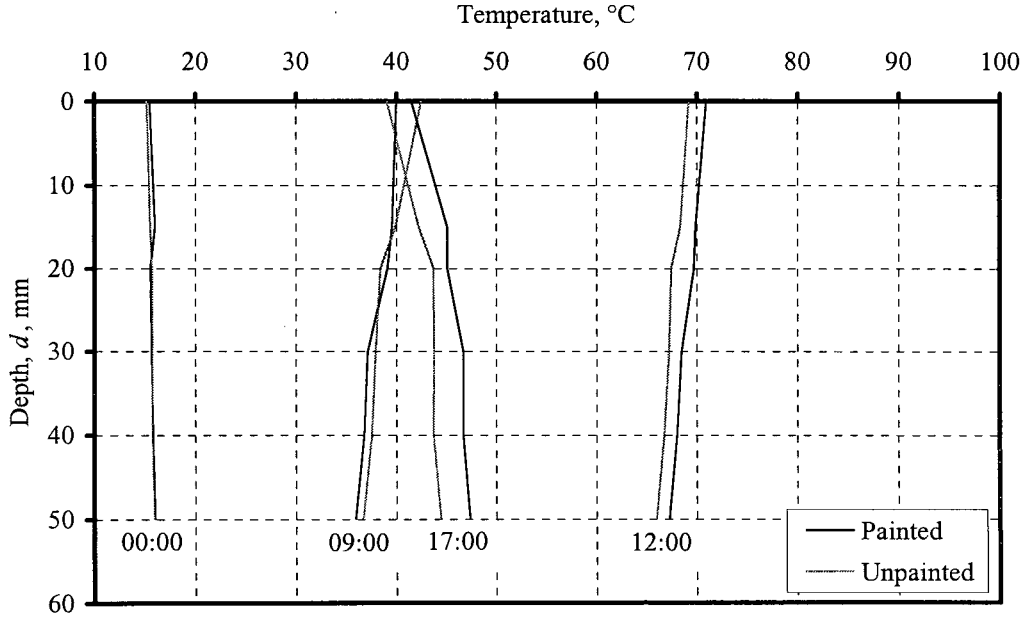

Figure 5.12: Temperature distribution at certain times on 14-03-2004 in the two mix B samples.

Figure 5.13 shows the net long wave radiation q_{rad}, convection q_{conv} and conduction q_{cond} heat fluxes on the surface of the painted mix A sample.

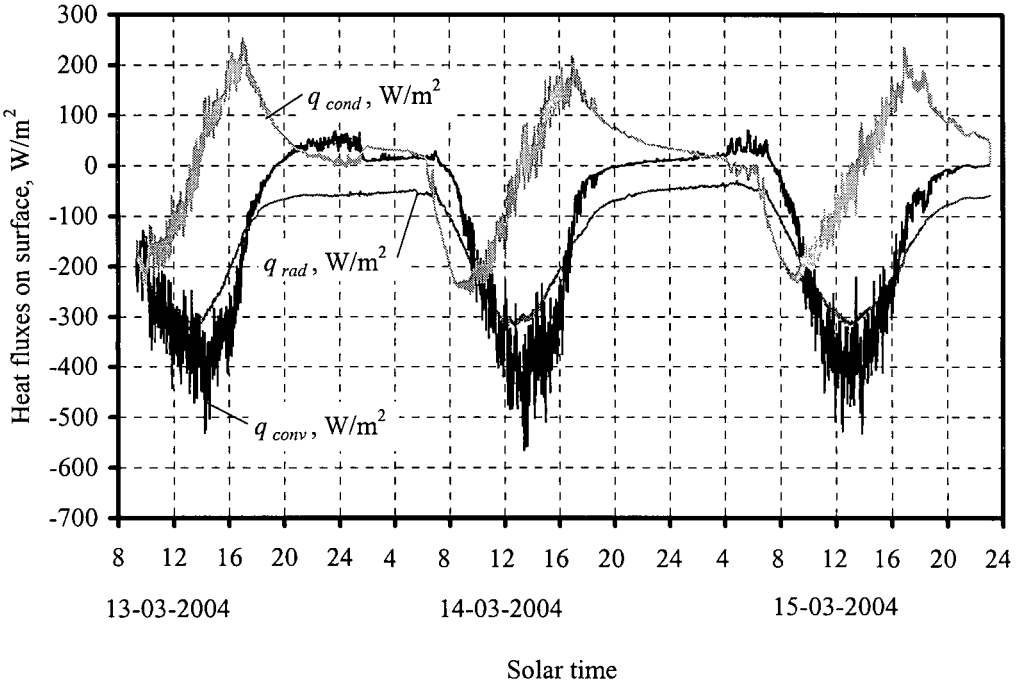

Figure 5.13: Heat fluxes on the surface of the painted mix A sample.

5.4 Simulation Model

The simulation model uses the ambient air temperature, wind speed, diffuse solar radiation, beam solar radiation, barometric pressure and dew point temperature data taken every minute as input data. The thermophysical properties of dry air are calculated with the correlations given by Kröger (2004), while the clear sky emissivity ε_{sky}, used in the calculation of the long wave radiation, is calculated with equations (2.6) and (2.7) and the convection heat transfer coefficient, used in the calculation of the convective heat transfer, is calculated with equations (3.10) and (4.5).

For the calculation of the pavement temperature at different depths, equations (5.7), (5.8), (5.10) and (5.11) are used. A control volume thickness Δt_g of 5 mm is used with a time step size Δt of 10 seconds.

The measured temperatures at 9:20 on the 13-03-2004 were used as initial temperatures for each control volume at the start of the simulation. The temperature for each control volume is then calculated iteratively until the energy balance for each control volume is satisfied.

5.5 Results and Discussion

Figures 5.14 to 5.17 shows the measured surface temperature and the temperature at a depth of 60 mm for each of the mix A samples compared with the calculated temperature over a period of time using the simulation model. From figures 5.11 and 5.12 it can be seen that there's not a big temperature gradient within the sample so it was decided to show the temperature only at these two nodes. In figure 5.9 it can be seen that the surface temperature of the painted sample, with its higher solar absorptivity, gets warmer than the unpainted sample during daytime. This can also be seen in the results of the simulation program.

The comparison of the results at depth seems to be more accurate than the results at the surface. This could be the effect of small temperature measurements errors at the surface due to the difficulty in connecting the thermocouple on the surface of the sample.

Figure 5.18 to 5.21 shows the measured surface temperature and the temperature at a depth of 50 mm for each of the mix B samples compared with the calculated temperature over the same time period using the simulation model.

The temperatures in the mix A samples is lower than the temperatures in the mix B samples due to the difference in diffusivity and the difference in the thickness of the samples.

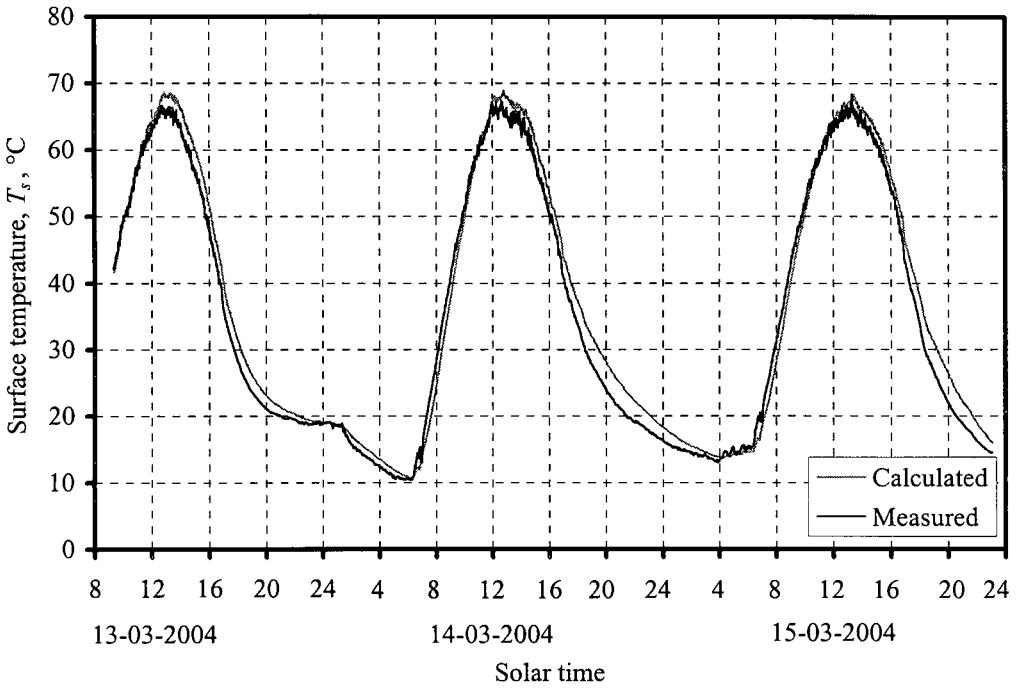

Figure 5.14: Measured and calculated surface temperature of the painted mix A sample.

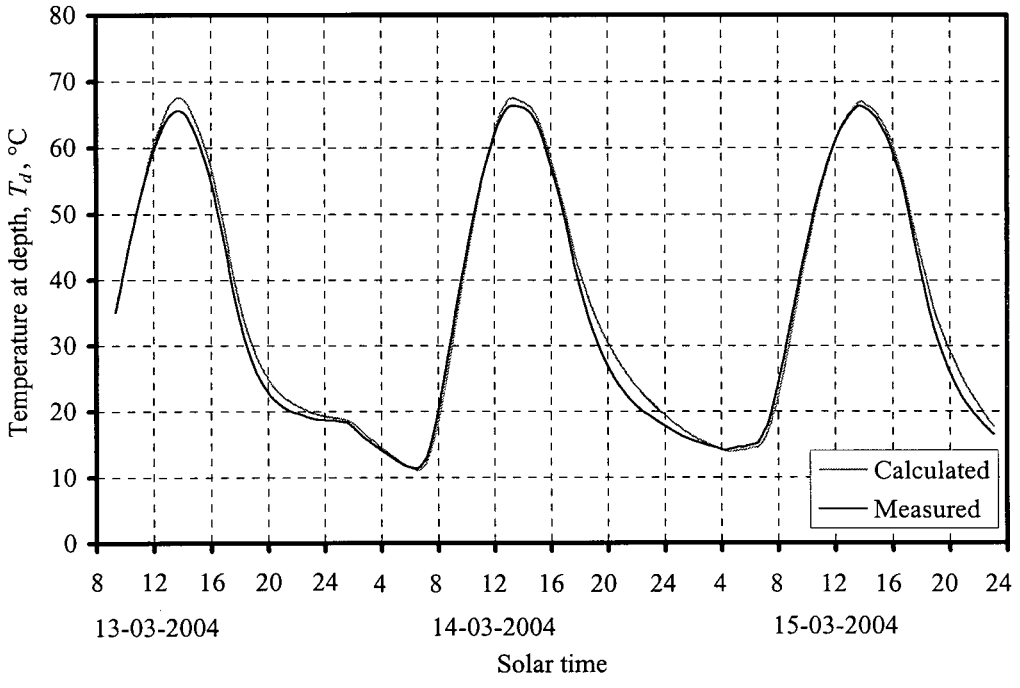

Figure 5.15: Measured and calculated temperature at a depth of 60 mm of the painted mix A sample.

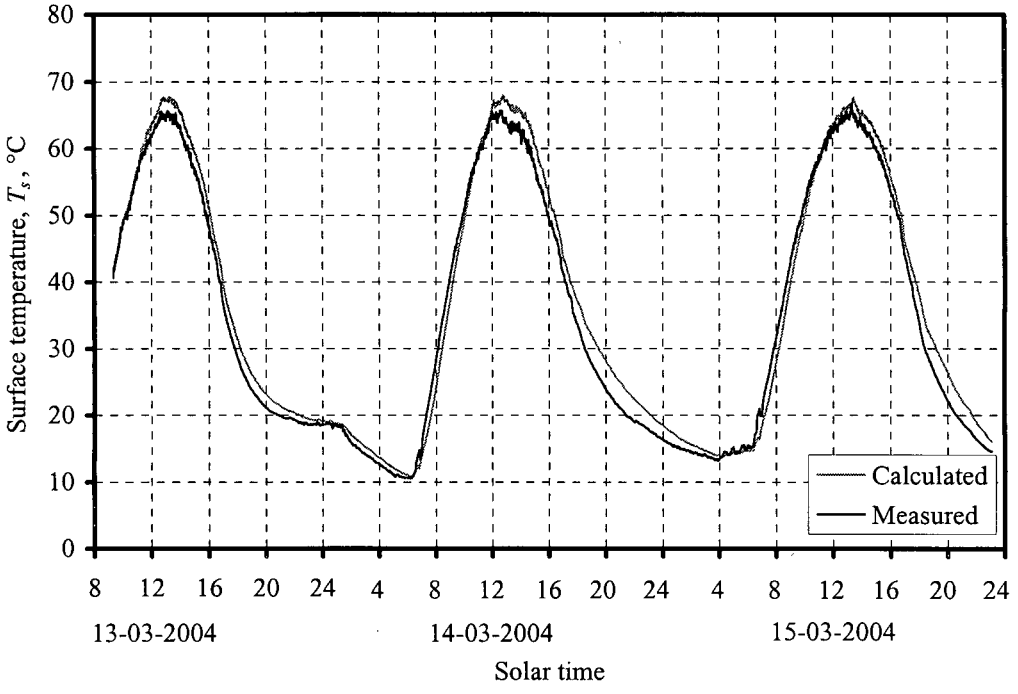

Figure 5.16: Measured and calculated surface temperature of the unpainted mix A sample.

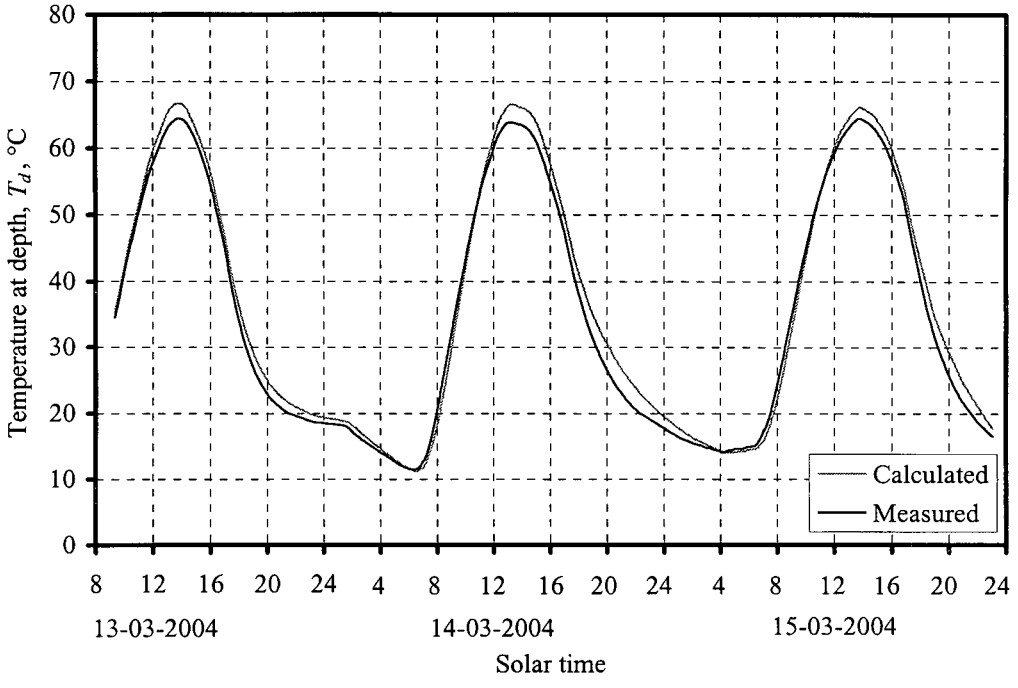

Figure 5.17: Measured and calculated temperature at a depth of 60 mm of the unpainted mix A sample.

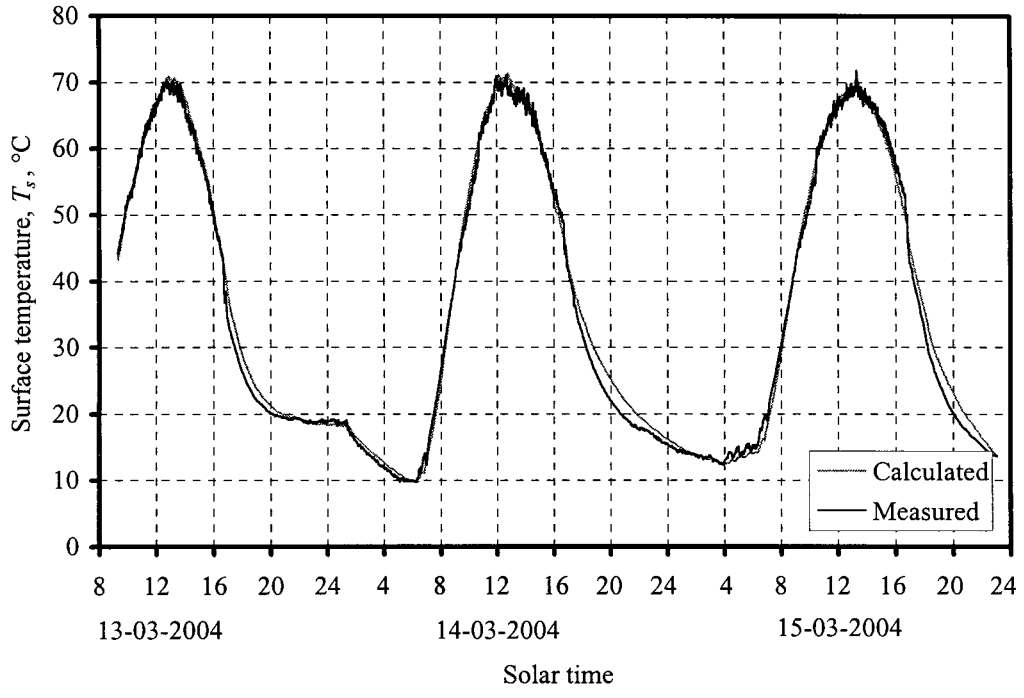

Figure 5.18: Measured and calculated surface temperature of the painted mix B sample.

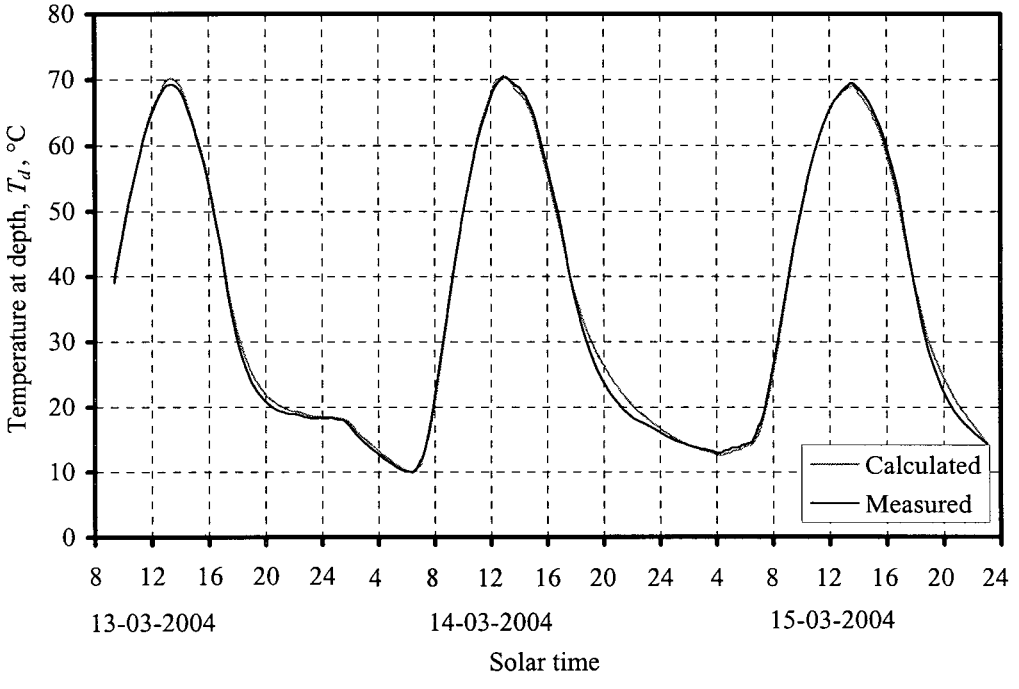

Figure 5.19: Measured and calculated temperature at a depth of 50 mm of the painted mix B sample.

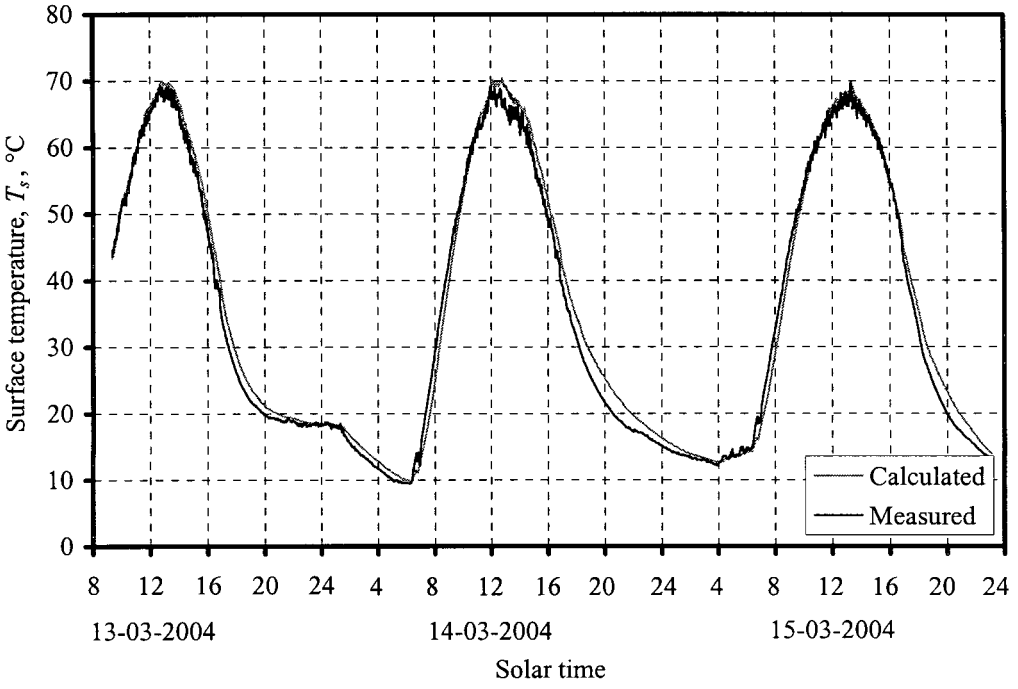

Figure 5.20: Measured and calculated surface temperature of the unpainted mix B sample.

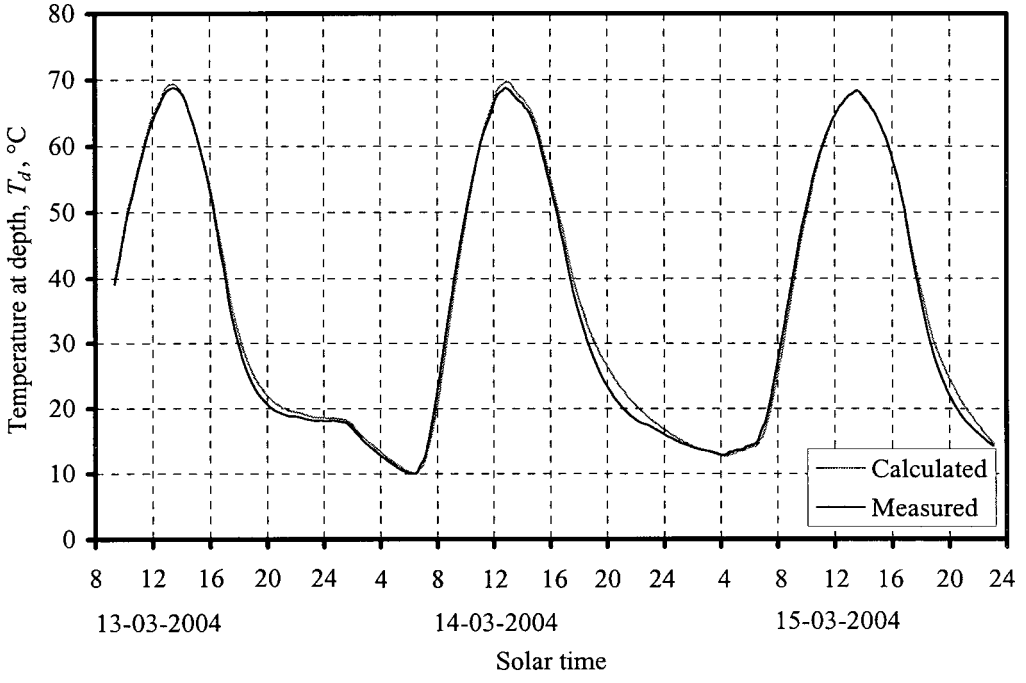

Figure 5.21: Measured and calculated temperature at a depth of 50 mm of the unpainted mix B sample.

The measured average maximum surface temperature $T_{s(max)}$ of each sample for the three days is shown in table 5.1 and compared with the values of the simulation model

Table 5.1: Average maximum surface temperature.

	Painted mix A sample	**Unpainted mix A sample**	**Painted mix B sample**	**Unpainted mix B sample**
Measured	67.475 °C	65.944 °C	70.913 °C	69.342 °C
Simulation model	67.128 °C	66.320 °C	68.807 °C	68.007 °C

As can be seen from table 5.1, the simulation model gives good results for the maximum surface temperature for all the samples.

The temperature distribution in the asphalt pavement is sensitive to the thermal properties of the pavement aggregate and asphalt. Figure 5.22 shows the measured and calculated surface temperature of the painted mix A asphalt sample using a diffusivity α_g of 6.084×10^{-7} m/s^2, as determined experimentally in Appendix E, in the simulation model. If compared with figure 5.14, which was calculated with a diffusivity of 6.94×10^{-7} m/s^2, it can be seen that the simulation results differ slightly with different diffusivity values. Figure 5.23 shows the difference in surface temperature, according to the simulation model, with a difference in diffusivity values. It is thus necessary to have the correct thermal properties for each layer of a pavement to predict the temperature distribution accurately.

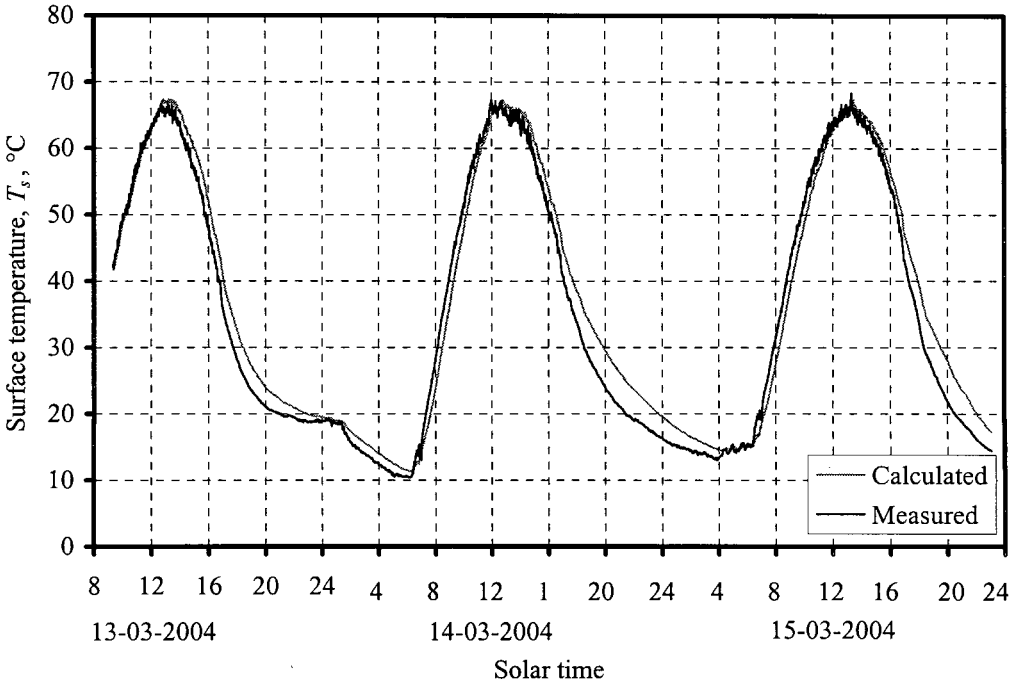

Figure 5.22: Measured and calculated surface temperature of the painted mix A sample (α_g = 6.084×10^{-7} m/s^2).

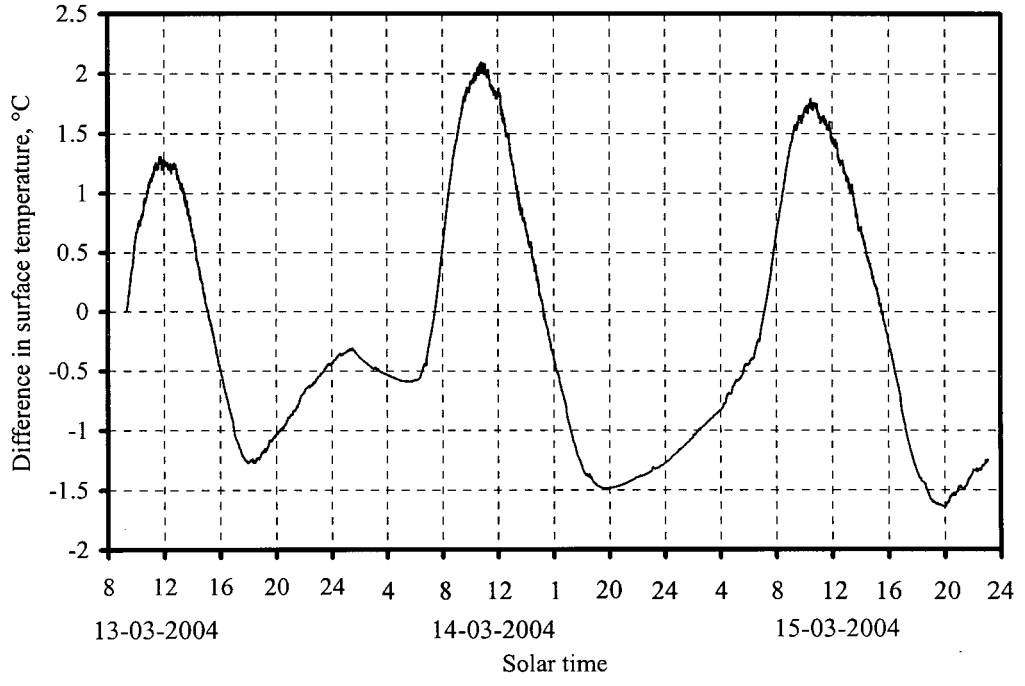

Figure 5.23: Difference in surface temperature for different diffusivity values ($\alpha_g = 6.084 \times 10^{-7}$ m/s^2 and $\alpha_g = 6.94 \times 10^{-7}$ m/s^2).

The temperatures at a depth of 60 mm for the mix A samples and 50 mm for the mix B samples were calculated with equation (5.3). Table 5.2 shows the comparison of the measured temperatures at depth, at the time of maximum surface temperature, for the four samples compared with the simulation model and equation (5.3). For the calculations using equation (5.3), the experimentally measured surface temperatures were used.

Table 5.2: Average temperature at depth.

	Painted mix A sample	**Unpainted mix A sample**	**Painted mix B sample**	**Unpainted mix B sample**
Measured	63.618 °C	61.746 °C	68.163 °C	67.080 °C
Simulation model	66.907 °C	66.068 °C	69.303 °C	68.476 °C
Equation (5.3)	67.462 °C	65.931 °C	70.901 °C	69.331 °C

The simulation model and equation (5.3) both give good results, but for equation (5.3) one has to have the value of the surface temperature at that time.

The simulation model was also used to predict the surface temperatures in a 100 mm, 200 mm and 300 mm thick asphalt pavements with the same aggregate gradations as the mix A and mix B asphalt samples. This was done in order to compare the results from the simulation model with equations (5.1), (5.2) and (5.4) used for estimating real pavement temperatures. These results are shown in table 5.3.

Superpave uses a convection heat transfer coefficient of h = 19.88 W/m^{2}K with the use of equation (5.1), while equation (5.4) uses the equation of Vehrencamp (1953) for the calculation of the convection heat transfer coefficient.

Table 5.3: Average maximum surface temperature.

	Painted mix A sample	**Unpainted mix A sample**	**Painted mix B sample**	**Unpainted mix B sample**
Simulation model	67.128 °C	66.320 °C	68.807 °C	68.007 °C
Simulation model (100 mm)	61.570 °C	61.255 °C	63.001 °C	62.059 °C
Simulation model (200 mm)	58.928 °C	57.864 °C	58.888 °C	58.480 °C
Simulation model (300 mm)	58.752 °C	58.730 °C	58.508 °C	58.193 °C
Equation (5.1)	55.338 °C	54.874 °C	53.519 °C	53.042 °C
Equation (5.2)	45.740 °C	45.740 °C	45.740 °C	45.740 °C
Equation (5.4)	76.621 °C	75.175 °C	76.947 °C	75.972 °C

Figures 5.24 and 5.25 show the predicted pavement surface temperature according to the simulation model at different pavement thicknesses for the four pavement samples. At a pavement thickness of 200 mm to 300 mm, the results of the simulation model is more comparable with real pavements and equation (5.1) is in reasonable agreement with the simulation model. As shown in figure 5.26 a heat transfer coefficient of h = 19.88 W/m^{2}K as assumed in the Superpave model, corresponds to a wind speed of approximately 3 m/s as predicted by equation (3.10).

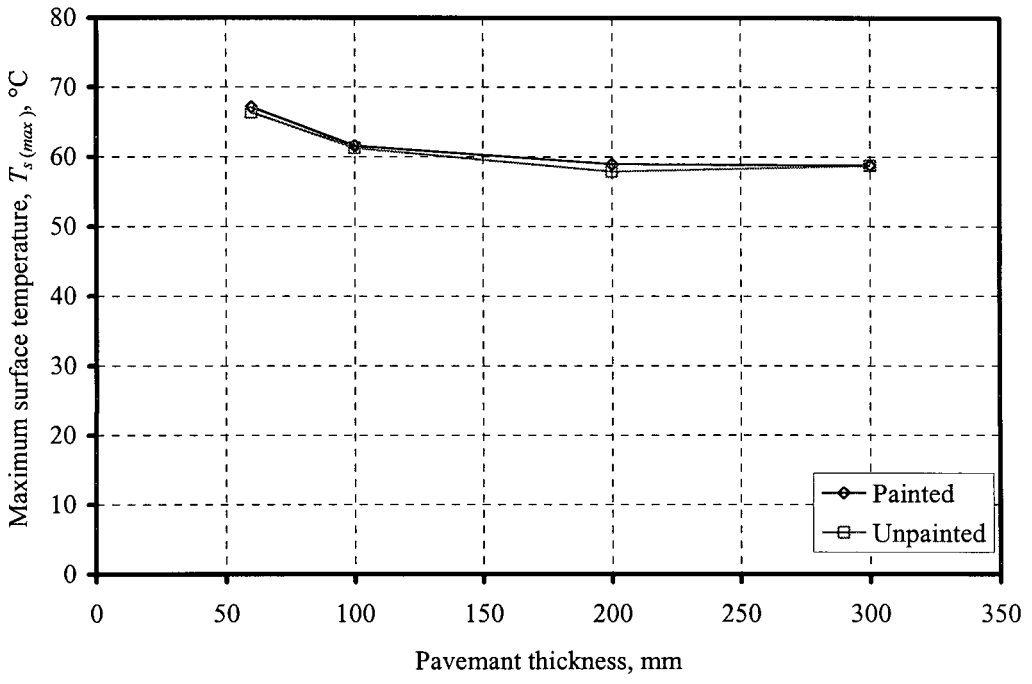

Figure 5.24: Predicted maximum pavement surface temperature of the two mix A samples at different pavement thicknesses.

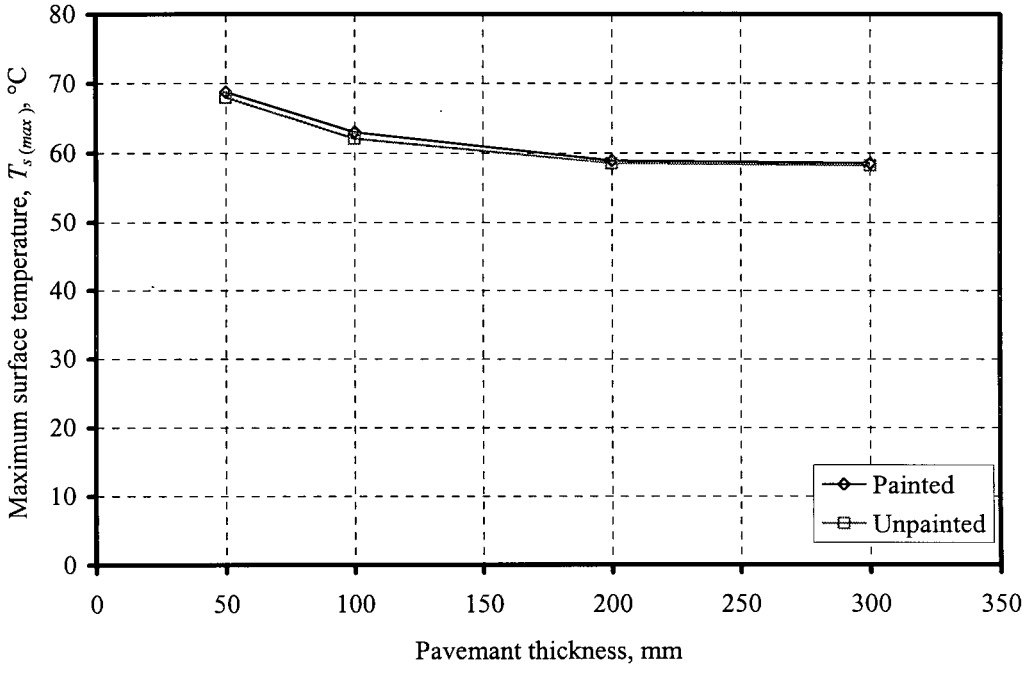

Figure 5.25: Predicted maximum pavement surface temperature of the two mix B samples at different pavement thicknesses.

As mentioned earlier, equation (5.4) uses the equation by Vehrencamp (1953) to calculate the convection heat transfer coefficient. It can be seen from figure 5.26 that the equation by Vehrencamp gives lower convection heat transfer coefficients than equation (3.10) used in the simulation model. This in part is the reason for higher predicted surface temperatures given by equation (5.4).

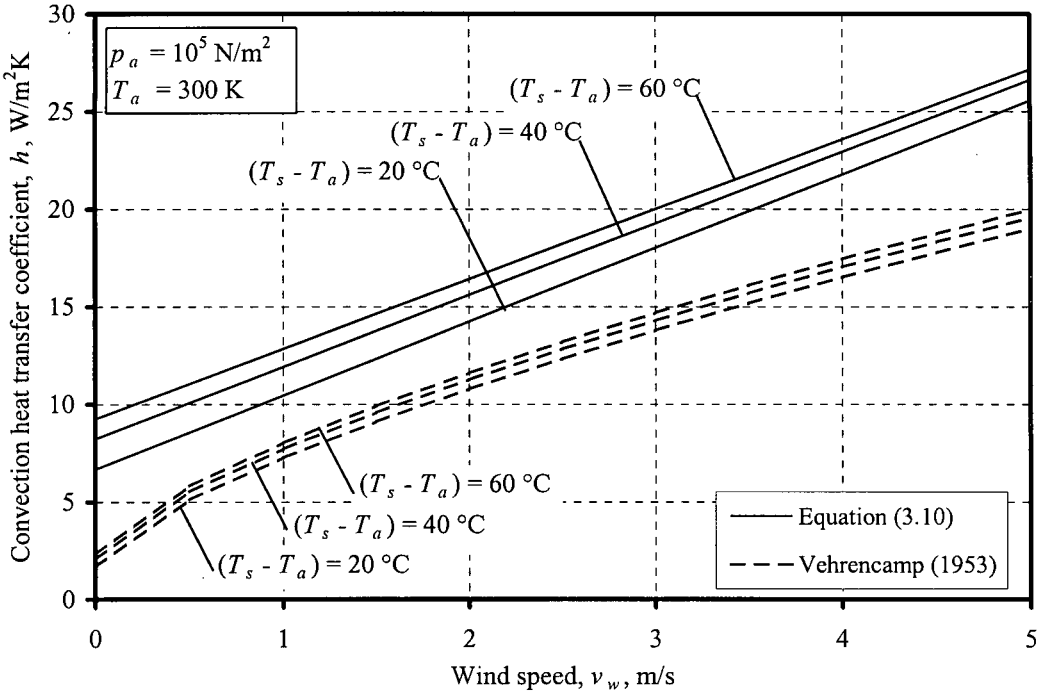

Figure 5.26: The convection heat transfer coefficient calculated with equation (3.10) and the equation by Vehrencamp (1953).

Equation (5.2) does not take into account the effect of wind speed, solar radiation or pavement thermal properties on pavement surface temperatures and therefore is too simplistic and does not give good results compared with the simulation model and equations (5.1) and (5.4).

A sample calculation for the calculation of the surface temperature and temperature at depth using equations (5.1) to (5.4) and the equations used in the simulation model is shown in Appendix D. For equations (5.1), (5.4) and the equations used in the simulation model only the last iteration is shown.

5.6 Conclusion

The convection heat transfer coefficients for the case where a surface is warmer than the ambient air (equation (3.10)) and for the case where a surface is cooler than the ambient air (equation (4.5)) were successfully used to predict the pavement surface temperature and the pavement temperature at depth with the use of a simulation model.

Conclusion

A simulation model was developed to predict the surface temperature and the temperature at depth of asphalt samples and pavements. Two new equations for calculating the convection heat transfer coefficient for periods when a horizontal surface is warmer than the ambient air and for periods when a surface is colder than the ambient air are used in the simulation model. The simulation model was successfully used to predict the surface temperature and temperature at depth of four asphalt pavement samples that were exposed to the natural environment.

The results of the simulation model were also compared with other correlations in the literature used to predict maximum pavement temperatures and temperatures at depth. Some of the correlations are in reasonable agreement with results predicted by the simulation model, but there are discrepancies, primarily due to limitations of and inherent simplifications in these equations.

References

1. Al-Arabi, M. and El-Riedy, M.K., Natural Convection Heat Transfer from Isothermal Horizontal Plates of Different Shapes, Int. Journal of Heat and Mass Transfer, 1976, vol. 19, pp. 1399 – 1404.

2. Bejan, A., Convection Heat Transfer, John Wiley & Sons, New York, 1984.

3. Berdahl, P. and Fromberg, R., The Thermal Radiance of Clear Skies, Solar Energy, 1982, vol. 32, no. 5, pp. 299 – 314.

4. Berger, X., Buriot, D. and Garnier, F., About the Equivalent Radiative Temperature For Clear Skies, Solar Energy, 1984, vol. 32, no. 6, pp. 725 – 733.

5. Bliss, R.A., Atmospheric Radiation Near the Surface of the Ground: A Summary for Engineers, Solar Energy, 1961, vol. 5, pp. 103 – 120.

6. Clark, G. and Allen C.P., The Estimation of Atmospheric Radiation for Clear Skies, Proceedings of the Second National Passive Solar Conference, Philadelphia, 1978, Part 2, p. 676.

7. Clausing, A.M. and Berton, J.J., An Experimental Investigation of Natural Convection from an Isothermal Horizontal Plate, Trans. of the ASME, Journal of Heat Transfer, 1989, III, pp. 904 – 908.

8. Duffie, J.A. and Beckman, W.A., Solar Engineering of Thermal Processes, Second Edition, John Wiley & Sons, Inc., New York, 1991.

9. Everitt, P.R., Dunbar, R., Swart, G. and Rossman, D., Current Pavement Temperature Monitoring in South Africa and its Applicability to Superpave and FWD Requirements, 7th Conference on Asphalt Pavements for South Africa, 1999.

10. Fujii, T. and Imura, H., Natural Convection Heat Transfer from a Plate with Arbitrary Inclination, Int. Journal of Heat and Mass Transfer, 1972, vol. 15, pp. 755 – 767.

11. Hermansson, Å., Mathematical Model for Paved Surface Summer and Winter Temperature: Comparison of Calculated and Measured Temperatures, Cold Regions Science and Technology, 2004, vol. 40, no. 1 – 2, pp. 1 – 17.

12. Highter W.M. and Wall, D.J., Thermal Properties of Some Asphaltic Concrete Mixes, Transportation Research Record, 1984, no. 968, pp. 38 – 45.

13. Huber, G.A., Weather Database for the Superpave Mix Design System, Strategic Highway Research Program, National Research Council, Washington DC, 1994.

14. Kröger, D.G., Convection Heat Transfer Between a Horizontal Surface and the Natural Environment, R and D Journal of the South African Institute of Mechanical Engineering, November 2002, vol. 18, no. 3, pp. 49 – 53.

15. Kröger, D.G., Air-Cooled Heat Exchangers and Cooling Towers, Thermal-Flow Performance and Evaluation and Design, Penn Well Corp., Tulsa, 2004.

16. Lloyd, J.R. and Moran, W.R., Natural Convection Adjacent to Horizontal Surfaces of Various Planforms, Trans. of the ASME, Journal of Heat Transfer, 1974, vol. 96, pp. 443 – 447.

17. Lombaard, I.F. and Kröger D.G., Heat Transfer Between a Horizontal Surface and the Natural Environment, Proc. ISES Conference, 2001, Adelaide.

18. Martin, M. and Berdahl, P., Characteristics of Infrared Sky Radiation in the United States, Solar Energy, 1984, vol. 33, pp. 321 – 336.

19. Mills, A.F., Heat and Mass Transfer, Richard D Irwin, inc., 1995.

20. Modest, M.F., Radiative Heat Transfer, McGraw-Hill, inc., 1993.

21. Rohsenow, W.M., Hartnett, J.P. and Cho, T.I., Handbook of Heat Transfer, McGraw Hill, New York, 1998.

22. Solaimanian, M. and Kennedy, T.W., Predicting Maximum Pavement Surface Temperatures Using Maximum Air Temperature and Hourly Solar Radiation, Transportation Research Record, 1993, no. 1417, pp. 1 – 11.

23. Swinbank, W.C., Long-wave Radiation from Clear Skies, Quarterly Journal Royal Meteorological Society, 1963, vol. 89, pp. 339 – 384.

24. Tang, R., Etzion, Y. and Meir, I.A., Estimates of Clear Sky Emissivity in the Negev Highlands, Israel, Energy Conversion & Management, 2004, vol. 45, pp.1831 – 1843.

25. Test, F.L., Lessmann, R.C. and Johary, A., Heat Transfer During Wind Flow over Rectangular Bodies in the Natural Environment, Trans. of the ASME, Journal of Heat Transfer, May 1981, vol. 103, pp. 262 – 267.

26. Vehrencamp, J.E., Experimental Investigation of Heat Transfer at an Air-Earth Interface, Trans, American Geophysical Union, 1953, vol. 34, no. 1, pp. 22 – 29.

27. Watmuff, J.H., Charter, W.W.S. and Proctor, D., Solar and Wind Induced External Coefficients Solar Collectors, Int. Revue d'Hellio-technique, 1977, vol. 2, no. 56.

Appendix A Determination of the Clear Sky Emissivity

Measured data at a standard time of 23:47 on 13 May 2004:

Surface temperatures:

T_{s1} = 8.953 °C T_{s2} = 9.140 °C T_{s3} = 9.065 °C T_{s4} = 8.516 °C T_{s5} = 8.691 °C
T_{s6} = 8.840 °C T_{s7} = 8.951 °C

Ambient air temperatures at different elevations (mm) above surface:

T_{100} = 8.340 °C
T_{200} = 8.315 °C
T_{400} = 8.378 °C
$T_a = T_{1000}$ = 8.44 °C

Dew point temperature:

T_{dp} = 6.6 °C

Voltage:

V = 79.3 V

Mean surface temperature, T_s:

$$T_s = \frac{T_{s1} + T_{s2} + T_{s3} + T_{s4} + T_{s5} + T_{s6} + T_{s7}}{7}$$
$$= \frac{8.953 + 9.140 + 9.065 + 8.516 + 8.691 + 8.840 + 8.951}{7}$$
$$= 8.879 \text{ °C or } 282.029 \text{ K}$$

The power Q needed to heat the aluminium plate using equation (2.16):

$$Q = qA = V^2/R = 79.3^2/88.6 = 70.976 \text{ W}$$

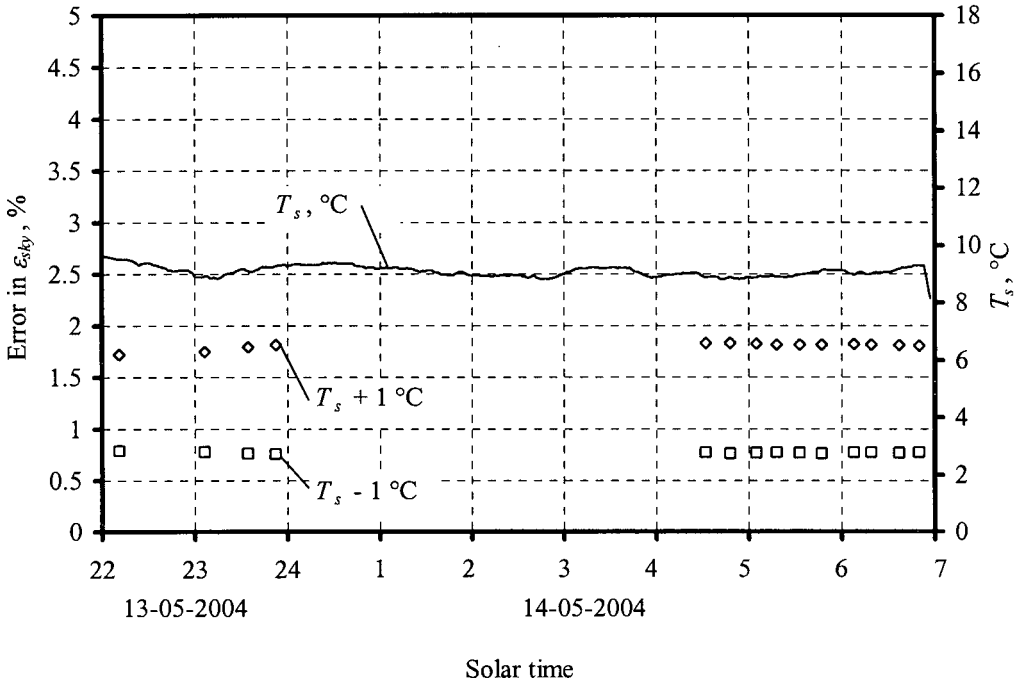

Figure A.1: Sensitivity of equation (2.15) to small temperature measurement errors.

Clear sky temperature T_{sky} using equation (2.15):

$$T_{sky} = \left(\frac{\varepsilon\sigma T_s^4 - q}{\alpha\sigma} \right)^{1/4} = \left(\frac{0.9 \times 5.67 \times 10^{-8} \times 282.029^4 - 70.976}{0.9 \times 5.67 \times 10^{-8}} \right)^{1/4} = 265.057 \; K$$

Clear sky emissivity ε_{sky} using equation (2.15):

$$\varepsilon_{sky} = (T_{sky}/T_a)^4 = (265.057/281.59)^4 = 0.785$$

Clear sky emissivity ε_{sky} using equation (2.6) by Berdahl and Fromberg (1982):

$$\begin{aligned}\varepsilon_{sky} &= 0.741 + 0.0062T_{dp} \\ &= 0.741 + 0.0062(6.6) \\ &= 0.782\end{aligned}$$

Figure A.1 shows that equation (2.15) gives a small error for a surface measurement error of ±1 °C.

Appendix B Sample Calculation for the Convection Heat Transfer Coefficient During Daytime

Location data (Stellenbosch, Western Cape, South Africa):

Altitude = 100 m

Latitude (° north of the equator): Φ = -33.93 °

Longitude (° west): L_{loc} = 341.15 °

Standard meridian: L_{st} = 330 °

Measured data at a local time of 13:19 on 29 January 2004:

Total hemispherical solar radiation:

I_h = 1066.728 W/m^2

Diffuse solar radiation:

I_d = 59.440 W/m^2

Surface temperatures:

$T_{s1} = 72.384$ °C $T_{s2} = 68.684$ °C $T_{s3} = 64.530$ °C
$T_{s4} = 71.102$ °C $T_{s5} = 69.480$ °C $T_{s6} = 66.873$ °C

Measured zenith angle at a local time of 13:15 on 29 January 2004:

$\theta_z = 15.255°$

Ambient air temperatures at different elevations (mm) above surface:

$T_{100} = 29.277$ °C
$T_{200} = 28.772$ °C
$T_{400} = 28.654$ °C
$T_a = T_{1000} = 27.573$ °C

Dew point temperature:

$T_{dp} = 9.96$ °C

Barometric pressure:

$p_a = 100576$ N/m^2

Relative humidity:

$\phi = 36$ %

Wind speed at different elevations (mm) above surface:

$v_{w@150} = 1.46$ m/s
$v_{w@1000} = 1.97$ m/s

Mean surface temperature, T_s:

$$T_s = \frac{T_{s1} + T_{s2} + T_{s3} + T_{s4} + T_{s5} + T_{s6}}{6}$$
$$= \frac{72.384 + 68.684 + 64.530 + 71.102 + 69.480 + 66.873}{6}$$
$$= 68.842\ ^\circ\text{C or } 341.992\ \text{K}$$

In general the wind speed distribution is close to the $1/7^{th}$ power law as shown in figure B.1.

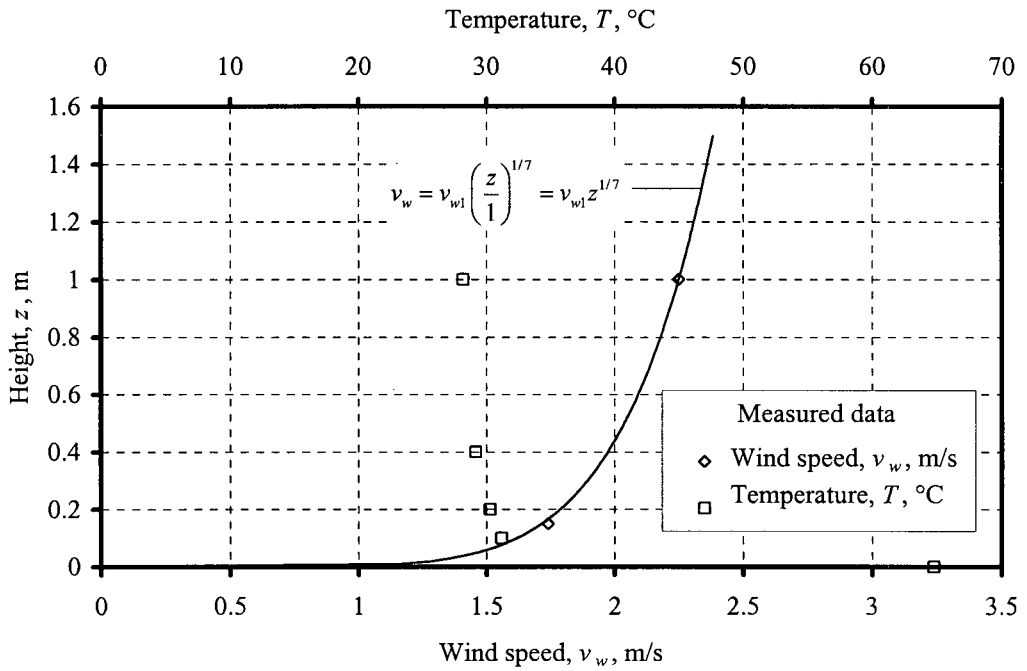

Figure B.1: The wind speed profile and temperature distribution at different heights above ground level.

Mean temperature between the surface and the ambient air, T_m:

$$T_m = \frac{T_s + T_a}{2} = \frac{341.992 + 300.723}{2} = 321.358\ \text{K}$$

Saturation pressure at T_a (Kröger (2004)):

$$z = 10.79586(1 - 273.16/T_a) + 5.02808 \log_{10}(273.16/T_a) + 1.50474 \times 10^{-4}[1 - 10^{-8.29692[(Ta/273.16) - 1]}] + 4.2873 \times 10^{-4}[10^{4.76955(1 - 273.16/Ta)} - 1] + 2.786118312$$

$$= 10.79586(1 - 273.16/300.723) + 5.02808 \log_{10}(273.16/300.723) + 1.50474 \times 10^{-4}[1 - 10^{-8.29692[(300.723/273.16) - 1]}] + 4.2873 \times 10^{-4}[10^{4.76955(1 - 273.16/300.723)} - 1] + 2.786118312$$

$$= 3.5666$$

$$p_{sat@Ta} = 10^z = 10^{3.5666} = 3686.378 \text{ N/m}^2$$

Vapour pressure at T_a:

$$p_v = \phi p_{sat@Ta} = 0.36 \times 3686.378 = 1327.096 \text{ N/m}^2$$

Calculated dew point temperature:

$$T_{dp} = 164.630366 + 1.832295 \times 10^{-3} p_v + 4.27215 \times 10^{-10} p_v^2 + 3.738954 \times 10^3 p_v^{-1} - 7.01204 \times 10^5 p_v^{-2} + 16.161488 \ln p_v - 1.437169 \times 10^{-4} p_v \ln p_v$$

$$= 164.630366 + 1.832295 \times 10^{-3}(1327.096) + 4.27215 \times 10^{-10}(1327.096)^2 + 3.738954 \times 10^3(1327.096)^{-1} - 7.01204 \times 10^5(1327.096)^{-2} + 16.161488 \ln(1327.096) - 1.437169 \times 10^{-4}(1327.096) \ln(1327.096)$$

$$= 284.324 \text{ K or } 11.174 \text{ °C}$$

This value is close to the value of 9.96 °C measured by the weather station.

Clear sky emissivity using equation (2.7):

$$\varepsilon_{sky} = 0.727 + 0.0060 T_{dp} = 0.727 + 0.0060(9.96) = 0.787$$

Sky temperature using equation (3.5):

$$T_{sky} = [\varepsilon_{sky} T_a^4]^{1/4} = [0.787(300.723)^4]^{1/4} = 283.244 \text{ K}$$

Thermophysical properties of dry air at T_m (Kröger (2004)):

Density:

$$\rho_a = \frac{p_a}{RT_m} = \frac{100576}{287.08 \times 321.358} = 1.090 \text{ kg/m}^3$$

Specific heat:

$$\begin{aligned} c_{pa} &= 1.045356 \times 10^3 - 3.161783 \times 10^{-1} T_m + 7.083814 \times 10^{-4} T_m^2 - 2.705209 \times 10^{-7} T_m^3 \\ &= 1.045356 \times 10^3 - 3.161783 \times 10^{-1} (321.358) + 7.083814 \times 10^{-4} (321.358)^2 \\ &\quad -2.705209 \times 10^{-7} (321.358)^3 \\ &= 1007.927 \text{ J/kgK} \end{aligned}$$

Dynamic viscosity:

$$\begin{aligned} \mu_a &= 2.287973 \times 10^{-6} + 6.259793 \times 10^{-8} T_m - 3.131956 \times 10^{-11} T_m^2 + 8.15038 \times 10^{-15} T_m^3 \\ &= 2.287973 \times 10^{-6} + 6.259793 \times 10^{-8} (321.358) - 3.131956 \times 10^{-11} (321.358)^2 \\ &\quad + 8.15038 \times 10^{-15} (321.358)^3 \\ &= 19.44 \times 10^{-6} \text{ kg/ms} \end{aligned}$$

Thermal conductivity:

$$\begin{aligned} k_a &= -4.937787 \times 10^{-4} + 1.0180878 \times 10^{-4} T_m - 4.627937 \times 10^{-8} T_m^2 + 1.250603 \times 10^{-11} T_m^3 \\ &= -4.937787 \times 10^{-4} + 1.0180878 \times 10^{-4} (321.358) - 4.627937 \times 10^{-8} (321.358)^2 \\ &\quad + 1.250603 \times 10^{-11} (321.358)^3 \\ &= 0.02786 \text{ W/mK} \end{aligned}$$

Angular dependence of solar absorptance:

To calculate the zenith angle one first needs to convert standard time to solar time and to do this, one needs to apply two corrections. Firstly a correction is required for the difference in longitude of the location L_{loc} in question and the standard meridian L_{st} for the local time zone. The second correction involves the equation of time *EOT*, which takes into account the perturbations in the earth's rate of rotation, which affects the time when the sun crosses the local longitude. The solar time can be calculated by using the following formula (Duffie and Beckman (1991)):

$$\text{Solar time} = \text{Standard time} + \frac{4(L_{st} - L_{loc}) + EOT}{60} \tag{B.1}$$

Equation of time *EOT* in minutes (Duffie and Beckman (1991)):

$$B = (n-1)\frac{360}{365} = (29-1)\frac{360}{365} = 27.616\ ^\circ$$

where n is the day of the year, which in this case is 29.

$$\begin{aligned} EOT &= 229.2[0.000075 + 0.001868\cos B - 0.032077\sin B - 0.014615\cos 2B \\ &\quad - 0.04089\sin 2B] \\ &= 229.2[0.000075 + 0.001868\cos(27.616^\circ) - 0.032077\sin(27.616^\circ) \\ &\quad - 0.014615\cos(2\times 27.616^\circ) - 0.04089\sin(2\times 27.616^\circ)] \\ &= -12.620 \text{ minutes} \end{aligned}$$

Solar time from equation (B.1):

$$\begin{aligned} \text{Solar time} &= \text{Standard time} + \frac{4(L_{st} - L_{loc}) + EOT}{60} \\ &= 13.317 + \frac{4(330 - 341.15) + (-12.620)}{60} \\ &= 12.363 \text{ hours} \end{aligned}$$

The zenith angle θ_z, needed to calculate the solar absorptance α_z of beam radiation, is the angle of incidence of beam radiation on a horizontal surface and can be calculated using the following equation by Duffie and Beckman (1991):

$$\theta_z = \cos^{-1}(\cos\Phi \cos\delta \cos\omega + \sin\Phi \sin\delta) \tag{B.2}$$

where Φ is the latitude of the location, δ is the declination angle and ω is the hour angle.

The declination angle δ is the angular position of the sun at solar noon with respect to the plane of the equator, with north positive.

Declination angle, δ (Duffie and Beckman (1991)):

$$\delta = 23.45 \sin\left(360\frac{284+n}{365}\right) = 23.45 \sin\left(360\frac{284+29}{365}\right) = -18.298\ ^\circ$$

The hour angle ω is the angular displacement of the sun east or west of the local longitude due to the rotation of the earth on its axis at 15 ° per hour, with morning negative and afternoon positive.

Hour angle, ω (Duffie and Beckman (1991)):

$$\omega = 15(\text{Solar time} - \text{Solar noon}) = 15(12.363 - 12) = 5.445\ ^\circ$$

Zenith angle θ_z from equation (B.2):

$$\begin{aligned}\theta_z &= \cos^{-1}(\cos\Phi \cos\delta \cos\omega + \sin\Phi \sin\delta)\\ &= \cos^{-1}(\cos(-33.93\ ^\circ) \cos(-18.298\ ^\circ) \cos(5.445\ ^\circ) + \sin(-33.93\ ^\circ)\ \sin(-18.298\ ^\circ))\\ &= 16.37\ ^\circ\end{aligned}$$

This value is close to the measured value of 15.255 °.

Beam solar absorptance using equation (3.3) at a zenith angle of 16.37 °:

$$\begin{aligned}\alpha_z &= \alpha\left[1+2.0345\times10^{-3}\theta_z-1.99\times10^{-4}\theta_z^2+5.324\times10^{-6}\theta_z^3-4.799\times10^{-8}\theta_z^4\right]\\ &= 0.93\left[1+2.0345\times10^{-3}\left(16.37\,^\circ\right)-1.99\times10^{-4}\left(16.37\,^\circ\right)^2+5.324\times10^{-6}\left(16.37\,^\circ\right)^3\right.\\ &\quad\left.-4.799\times10^{-8}\left(16.37\,^\circ\right)^4\right]\\ &\approx 0.93\end{aligned}$$

Diffuse solar absorptance using equation (3.3) at an angle of 60 °:

$$\begin{aligned}\alpha_d &= \alpha\left[1+2.0345\times10^{-3}\theta_z-1.99\times10^{-4}\theta_z^2+5.324\times10^{-6}\theta_z^3-4.799\times10^{-8}\theta_z^4\right]\\ &= 0.93\left[1+2.0345\times10^{-3}\left(60\,^\circ\right)-1.99\times10^{-4}\left(60\,^\circ\right)^2+5.324\times10^{-6}\left(60\,^\circ\right)^3\right.\\ &\quad\left.-4.799\times10^{-8}\left(60\,^\circ\right)^4\right]\\ &= 0.8683\end{aligned}$$

Beam solar radiation I_b from equation (3.2):

$$\begin{aligned}I_b &= I_h - I_d\\ &= 1066.728 - 59.440\\ &= 1007.288\ \text{W/m}^2\end{aligned}$$

Mixed convection heat transfer coefficient using equation (3.6):

$$\begin{aligned}h &= \frac{I_b\alpha_z + I_d\alpha_d - \left(\varepsilon\sigma T_s^4 - \alpha_{lw}\sigma T_{sky}^4\right)}{T_s - T_a}\\ &= \frac{1007.288\times0.93+59.440\times0.8683-5.67\times10^{-8}\left(0.9\times341.992^4-0.9\times283.244^4\right)}{341.992-300.723}\\ &= 14.994\ \text{W/m}^2\text{K}\end{aligned}$$

Left-hand side of equation (3.10):

$$h\left[\frac{\mu T_m}{g(T_s - T_a)c_p k^2 \rho^2}\right]^{1/3}$$

$$= 14.994\left[\frac{19.44\times10^{-6}\times321.358}{9.81\times(341.992-300.723)\times1007.927\times0.02786^2\times1.090^2}\right]^{1/3}$$

$$= 0.3825$$

Right-hand side of equation (3.10):

$$0.2106 + 0.0026 v_w\left[\frac{\rho T_m}{\mu g(T_s - T_a)}\right]^{1/3}$$

$$= 0.2106 + 0.0026\times1.97\left[\frac{1.090\times321.358}{19.44\times10^{-6}\times9.81\times(341.992-300.723)}\right]^{1/3}$$

$$= 0.3921$$

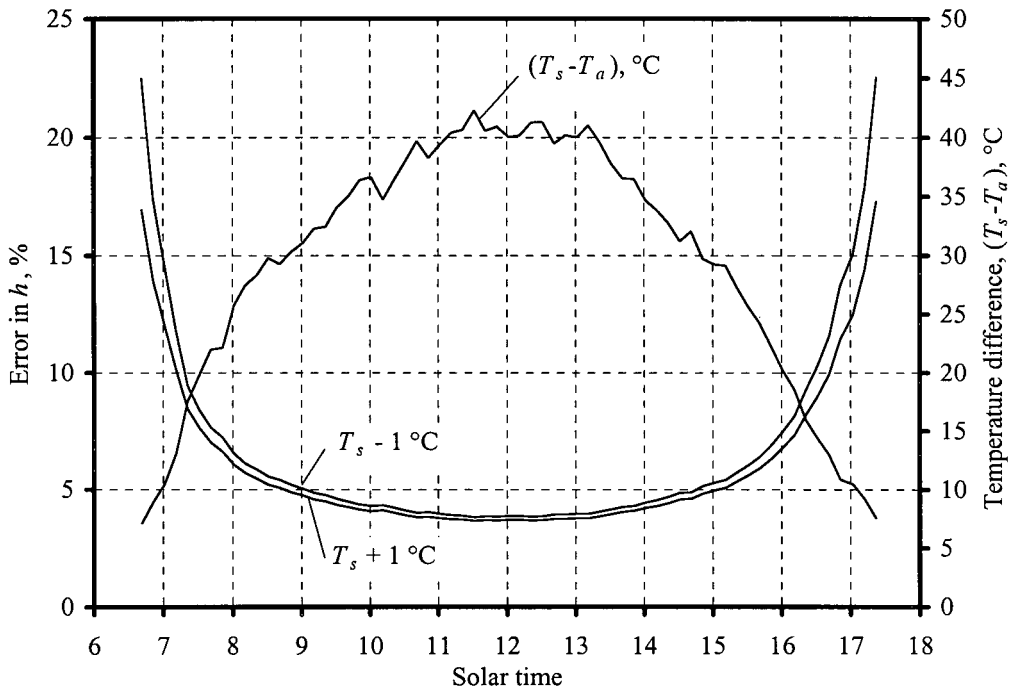

Figure B.2: Sensitivity of equation (3.6) to small temperature measurement errors.

Only experimental data taken during the period 7:00 to 17:00 was considered since the nature of equation (3.6), used to evaluate the heat transfer coefficient, is such that it becomes very

sensitive to small errors in temperature measurement before and after these times, as is shown in figure B.2 for an error of ±1 °C in surface temperature.

Appendix C Sample Calculation for the Convection Heat Transfer Coefficient During Nighttime

Location data (Stellenbosch, Western Cape, South Africa):

Altitude = 100 m

Latitude (° north of the equator): Φ = -33.93 °

Longitude (° west): L_{loc} = 341.15 °

Standard meridian: L_{st} = 330 °

Measured data at a local time of 20:01 on 29 January 2004:

Surface temperatures:

T_{s1} = 18.459 °C T_{s2} = 18.848 °C T_{s3} = 19.167 °C

T_{s4} = 18.597 °C T_{s5} = 18.548 °C T_{s6} = 19.124 °C

Ambient air temperatures at different elevations (mm) above surface:

T_{100} = 22.321 °C

T_{200} = 22.345 °C

T_{400} = 22.404 °C

$T_a = T_{1000}$ = 22.491 °C

Dew point temperature:

$$T_{dp} = 11.5\ ^{\circ}\text{C}$$

Barometric pressure:

$$p_a = 100345\ \text{N/m}^2$$

Wind speed at different elevations (mm) above surface:

$$v_{w@150} = 2.14\ \text{m/s}$$
$$v_{w@1000} = 2.92\ \text{m/s}$$

Mean surface temperature, T_s:

$$T_s = \frac{T_{s1} + T_{s2} + T_{s3} + T_{s4} + T_{s5} + T_{s6}}{6}$$
$$= \frac{18.459 + 18.848 + 19.167 + 18.597 + 18.548 + 19.124}{6}$$
$$= 18.791\ ^{\circ}\text{C or } 291.941\ \text{K}$$

In general the velocity distribution is close to the $1/7^{th}$ power law as shown in figure C.1.

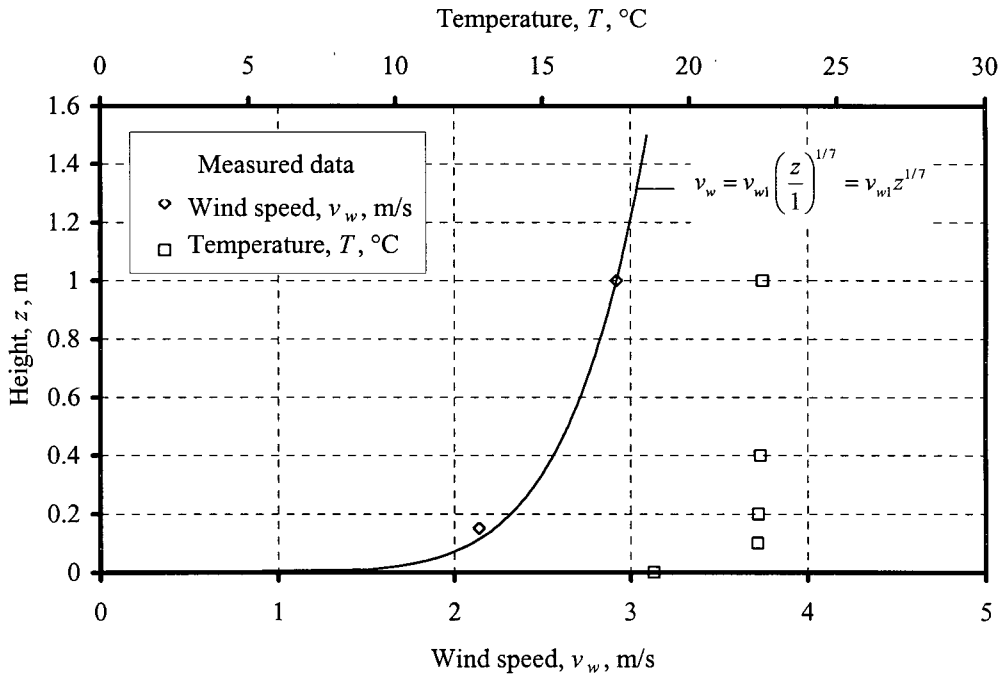

Figure C.1: The wind velocity profile and temperature distribution at different heights above ground level.

Mean temperature between the surface and the ambient air, T_m:

$$T_m = \frac{T_s + T_a}{2} = \frac{291.941 + 295.641}{2} = 293.791 \text{ K}$$

Clear sky emissivity using equation (2.6):

$$\varepsilon_{sky} = 0.741 + 0.0062 T_{dp} = 0.741 + 0.0062(11.5) = 0.812$$

Sky temperature using equation (3.5):

$$T_{sky} = [\varepsilon_{sky} T_a^4]^{1/4} = [0.812(295.641)^4]^{1/4} = 280.643 \text{ K}$$

Thermophysical properties of dry air at T_m (Kröger (2004)):

Density:

$$\rho_a = \frac{p_a}{RT_m} = \frac{100345}{287.08 \times 293.791} = 1.190 \text{ kg/m}^3$$

Specific heat:

$$\begin{aligned} c_{pa} &= 1.045356 \times 10^3 - 3.161783 \times 10^{-1} T_m + 7.083814 \times 10^{-4} T_m^{\,2} - 2.705209 \times 10^{-7} T_m^{\,3} \\ &= 1.045356 \times 10^3 - 3.161783 \times 10^{-1} (293.791) + 7.083814 \times 10^{-4} (293.791)^2 \\ &\quad -2.705209 \times 10^{-7} (293.791)^3 \\ &= 1006.748 \text{ J/kgK} \end{aligned}$$

Dynamic viscosity:

$$\begin{aligned} \mu_a &= 2.287973 \times 10^{-6} + 6.259793 \times 10^{-8} T_m - 3.131956 \times 10^{-11} T_m^{\,2} + 8.15038 \times 10^{-15} T_m^{\,3} \\ &= 2.287973 \times 10^{-6} + 6.259793 \times 10^{-8} (293.791) - 3.131956 \times 10^{-11} (293.791)^2 \\ &\quad +8.15038 \times 10^{-15} (293.791)^3 \\ &= 18.182 \times 10^{-6} \text{ kg/ms} \end{aligned}$$

Thermal conductivity:

$$\begin{aligned} k_a &= -4.937787 \times 10^{-4} + 1.0180878 \times 10^{-4} T_m - 4.627937 \times 10^{-8} T_m^{\,2} + 1.250603 \times 10^{-11} T_m^{\,3} \\ &= -4.937787 \times 10^{-4} + 1.0180878 \times 10^{-4} (293.791) - 4.627937 \times 10^{-8} (293.791)^2 \\ &\quad +1.250603 \times 10^{-11} (293.791)^3 \\ &= 0.02574 \text{ W/mK} \end{aligned}$$

Convection heat transfer coefficient using equation (4.2):

$$h = \frac{\left(\varepsilon\sigma T_s^4 - \alpha_{lw}\sigma T_{sky}^4\right)}{\left(T_a - T_s\right)}$$

$$= \frac{\left(0.9\times 5.67\times 10^{-8}\times 291.945^4 - 0.9\times 5.67\times 10^{-8}\times 280.643^4\right)}{\left(295.641 - 291.945\right)}$$

$$= 14.653 \text{ W/m}^2\text{K}$$

Convection heat transfer coefficient using equation (4.5):

$$h = 3.87 + 0.0022\frac{v_w \rho c_p}{\left(\mu c_p / k\right)^{2/3}}$$

$$= 3.87 + 0.0022\frac{2.92\times 1.190\times 1006.748}{\left(18.182\times 10^{-6}\times 1006.748/0.02574\right)^{2/3}}$$

$$= 13.531 \text{ W/m}^2\text{K}$$

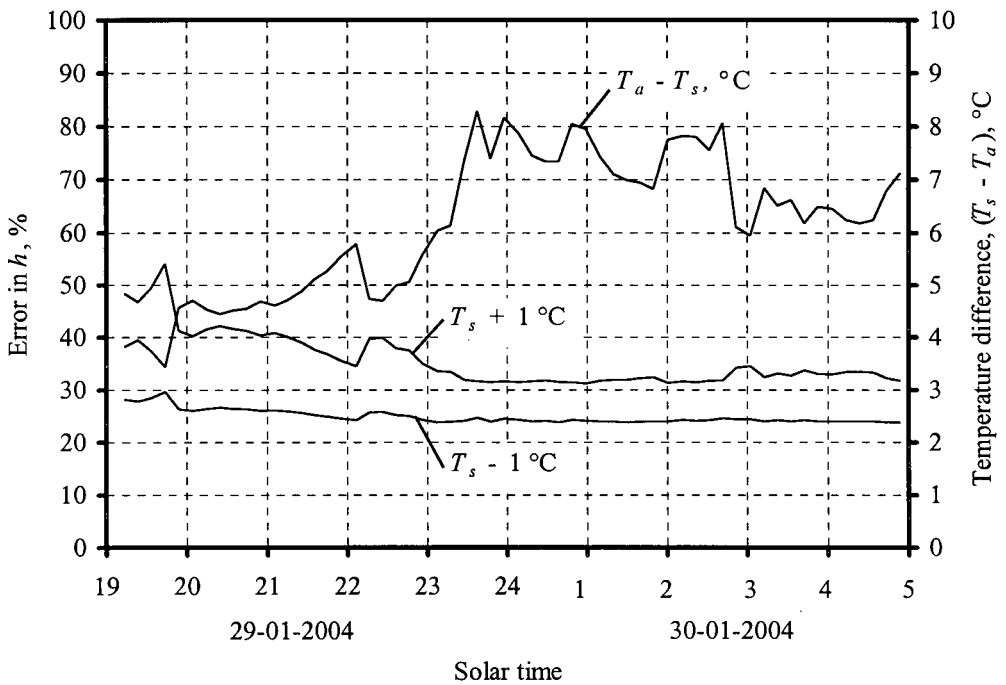

Figure C.2: Sensitivity of equation (4.2) to small temperature measurement errors.

During nighttime the temperature difference between the ambient air Ta and the surface Ts is relatively small and therefore equation (4.2) is very sensitive to small temperature measuring errors. This can be seen in figure C.2 for a measuring error of ±1 °C in surface temperature.

Appendix D Sample Calculation for the Prediction of Pavement Surface Temperature and Temperature at Depth

Measured data at a solar time of 12:44 on 13 March 2004:

Total hemispherical solar radiation:

$I_h = 893.827$ W/m^2

Diffuse solar radiation:

$I_d = 61.779$ W/m^2

Maximum surface temperature of the painted mix A sample:

$T_{s(max)} = 66.685$ °C

Temperature at a depth of 60 mm below the surface:

$T_d = 63.369$ °C

Ambient air temperature:

$$T_a = 33.076\ °C$$

Dew point temperature:

$$T_{dp} = 9.1\ °C$$

Barometric pressure:

$$p_a = 100860\ N/m^2$$

Wind speed at a height of 1 m above the surface:

$$v_w = 0\ m/s$$

Daytime clear sky emissivity using equation (2.7):

$$\varepsilon_{sky} = 0.727 + 0.0060T_{dp} = 0.727 + 0.0060(9.1) = 0.782$$

Sky temperature using equation (3.5):

$$T_{sky} = [\varepsilon_{sky} T_a^4]^{1/4} = [0.782 \times 306.226^4]^{1/4} = 287.968\ K$$

Calculation of the pavement surface temperature using equation (5.1):

Calculated surface temperature for the previous iteration:

$$T_s = 52.38\ °C$$

Radiation heat transfer coefficient used for linearising equation (5.1):

$$h_r = \varepsilon\sigma T_s^3 = 0.9 \times 5.67 \times 10^{-8}(52.38 + 273.15)^3 = 1.76 \text{ W/m}^2\text{K}$$

Surface temperature by rearranging equation (5.1) with $h = 19.88$ W/m^{2}K:

$$T_s = \frac{1331\alpha\tau_a^{1/\cos\Phi}\cos\Phi + \varepsilon_{sky}\sigma T_a^4 + hT_a - 164k}{h + h_r}$$

$$= [1331 \times 0.93 \times 0.81^{1/\cos(-33.93)}\cos(-33.93) + 0.782 \times 5.67 \times 10^{-8}(33.076 + 273.15)^4$$
$$+ 19.88(33.076 + 273.15) - 164 \times 1.4]/(19.88 + 1.76)$$
$$= 325.535 \text{ K}$$
$$= 52.385 \text{ °C}$$

Calculation of the pavement surface temperature using equation (5.2):

$$T_s = T_a - 0.00618\Phi^2 + 0.2289\Phi + 24.4$$
$$= 33.076 - 0.00618(-33.93)^2 + 0.2289(-33.93) + 24.4$$
$$= 42.595 \text{ °C}$$

Calculation of the pavement temperature at a depth of 60 mm using equation (5.3) and the measured surface temperature of 66.685 °C:

$$T_d = (T_s + 17.8)(1 - 2.48 \times 10^{-3}d + 1.085 \times 10^{-5}d^2 - 2.441 \times 10^{-8}d^3) - 17.8$$
$$= (66.685 + 17.8)(1 - 2.48 \times 10^{-3}(0.06) + 1.085 \times 10^{-5}(0.06)^2 - 2.441 \times 10^{-8}(0.06)^3)$$
$$- 17.8$$
$$= 66.672 \text{ °C}$$

Calculation of the pavement surface temperature using equation (5.4):

Calculated surface temperature for the previous iteration:

$$T_s = 78.332 \text{ °C}$$

Mean Temperature:

$$T_m = \frac{T_s + T_a}{2} = \frac{78.322 + 33.076}{2} = 55.714\ ^\circ\text{C or } 328.854\ \text{K}$$

Radiation heat transfer coefficient used for linearising equation (5.4):

$$h_r = \varepsilon\sigma T_s^3 = 0.9 \times 5.67 \times 10^{-8}(78.332 + 273.15)^3 = 2.216$$

Convection heat transfer coefficient by Vehrencamp (1953):

$$\begin{aligned} h &= 698.24[0.00144 T_m^{0.3} v_w^{0.7} + 0.00097(T_s - T_a)^{0.3}] \\ &= 698.24[0.00144(328.854)^{0.3}(0)^{0.7} + 0.00097(351.482 - 306.226)^{0.3}] \\ &= 2.126 \end{aligned}$$

Surface temperature by rearranging equation (5.4):

$$\begin{aligned} T_s &= \frac{1394\alpha\tau_a^{1/\cos\Phi}\cos\Phi + \varepsilon_{sky}\sigma T_a^4 + hT_a + kT_d/d}{h + h_r + k/d} \\ &= [1394 \times 0.93 \times 0.81^{1/\cos(-33.93)}\cos(-33.93) + 0.782 \times 5.67 \times 10^{-8}(33.076 + 273.15)^4 \\ &\quad + 2.126(33.076 + 273.15) + 1.4 \times (63.369 + 273.15)/0.06]/(2.126 + 2.216 + 1.4/0.06) \\ &= 351.485\ \text{K} \\ &= 78.335\ ^\circ\text{C} \end{aligned}$$

Calculating the pavement surface temperature using equation (5.7) used in the simulation model:

Calculated surface temperature for the previous iteration:

$$T_{g,0}^{\,i} = 68.192\ ^\circ\text{C}$$

Calculated temperature for the control volume 5 mm underneath the surface for the previous iteration:

$$T_{g,1}^{\,i} = 67.481\ ^\circ\text{C}$$

Calculated solar absorptance:

$$\alpha_s \approx 0.93$$

Mean temperature between the surface and the ambient air:

$$T_m = \frac{T_s + T_a}{2} = \frac{T_{g,0}^{\,i} + T_a}{2} = \frac{68.192 + 33.076}{2} = 50.634\ ^\circ\text{C or } 323.784\ \text{K}$$

Thermophysical properties of dry air at T_m (Kröger (2004)):

Density:

$$\rho_a = \frac{p_a}{RT_m} = \frac{100860}{287.08 \times 323.784} = 1.085\ \text{kg/m}^3$$

Specific heat:

$$\begin{aligned} c_{pa} &= 1.045356 \times 10^3 - 3.161783 \times 10^{-1} T_m + 7.083814 \times 10^{-4} T_m^{\,2} - 2.705209 \times 10^{-7} T_m^{\,3} \\ &= 1.045356 \times 10^3 - 3.161783 \times 10^{-1} (323.784) + 7.083814 \times 10^{-4} (323.784)^2 \\ &\quad -2.705209 \times 10^{-7} (323.784)^3 \\ &= 1008.064\ \text{J/kgK} \end{aligned}$$

Dynamic viscosity:

$$\begin{aligned}\mu_a &= 2.287973\times10^{-6} + 6.259793\times10^{-8}T_m - 3.131956\times10^{-11}T_m^{\,2} + 8.15038\times10^{-15}T_m^{\,3}\\ &= 2.287973\times10^{-6} + 6.259793\times10^{-8}(323.784) - 3.131956\times10^{-11}(323.784)^2\\ &\quad +8.15038\times10^{-15}(323.784)^3\\ &= 19.549\times10^{-6}\ \text{kg/ms}\end{aligned}$$

Thermal conductivity:

$$\begin{aligned}k_a &= -4.937787\times10^{-4} + 1.0180878\times10^{-4}T_m - 4.627937\times10^{-8}T_m^{\,2} + 1.250603\times10^{-11}T_m^{\,3}\\ &= -4.937787\times10^{-4} + 1.0180878\times10^{-4}(323.784) - 4.627937\times10^{-8}(323.784)^2\\ &\quad +1.250603\times10^{-11}(323.784)^3\\ &= 0.02804\ \text{W/mK}\end{aligned}$$

Convection heat transfer coefficient using equation (3.10):

$$\begin{aligned}h &= \left[0.2106 + 0.0026v_w\left[\frac{\rho T_m}{\mu g(T_s - T_a)}\right]^{1/3}\right]\left[\frac{g(T_s - T_a)c_p k^2\rho^2}{\mu T_m}\right]^{1/3}\\ &= \left[0.2106 + 0.0026\times0\left[\frac{1.085\times323.784}{19.549\times10^{-6}\times9.81(341.342 - 306.226)}\right]^{1/3}\right]\\ &\quad\times\left[\frac{9.81(341.342 - 306.226)1008.064\times0.02804^2\times1.085^2}{19.549\times10^{-6}\times323.784}\right]^{1/3}\\ &= 7.799\ \text{W/m}^2\text{K}\end{aligned}$$

Radiation heat transfer coefficient used for linearising equation (5.7):

$$\begin{aligned}h_r &= \varepsilon\sigma(T_s + T_{sky})(T_s^{\,2} + T_{sky}^{\,2})\\ &= \varepsilon\sigma((T_{g,0}^{\,i}) + T_{sky})((T_{g,0}^{\,i})^2 + T_{sky}^{\,2})\\ &= 0.9\times5.67\times10^{-8}(341.342 + 287.968)(341.342^2 + 287.968^2)\\ &= 6.405\ \text{W/m}^2\text{K}\end{aligned}$$

Surface temperature by rearranging equation (5.7):

$$T_{g,0}^{i+1} = \frac{\alpha_z I_b + \alpha_d I_d + hT_a + h_r T_{sky} + k_g T_{g,1}^i / \Delta z_1 + k_g \Delta l_{g,0} T_{g,0}^i / (\alpha_g \Delta t)}{h + h_r + k_g / \Delta z_1 + k_g \Delta l_{g,0} / (\alpha_g \Delta t)}$$

$$= \frac{\left[\begin{array}{l} 0.93 \times 832.048 + 0.8683 \times 61.779 + 7.799 \times 306.226 + 6.405 \times 287.968 \\ + 1.4 \times 340.631 / 0.0075 + 1.4 \times 0.005 \times 341.342 / (6.94 \times 10^{-7} \times 10) \end{array}\right]}{7.799 + 6.405 + 1.4 / 0.0075 + 1.4 \times 0.005 / (6.94 \times 10^{-7} \times 10)}$$

$$= 341.407 \text{ K or } 68.257 \text{ °C}$$

Calculation of the pavement temperature at a depth of 60 mm using equation (5.12) used by the simulation model:

Calculated temperature at a depth of 60 mm for the last iteration:

$$T_{g,N}^{i} = 64.474 \text{ °C}$$

Calculated temperature for the control volume 5 mm above the bottom of the pavement for the current iteration:

$$T_{g,N-1}^{i+1} = 64.476 \text{ °C}$$

Temperature at a depth of 60 mm by rearranging equation (5.12):

$$T_{g,N}^{i+1} = \frac{k_g T_{g,N-1}^{i+1} / \Delta z_N + k_g \Delta l_{g,N} T_{g,N}^i / (\alpha_g \Delta t)}{k_g / \Delta z_N + k_g \Delta l_{g,N} / (\alpha_g \Delta t)}$$

$$= \frac{1.4 \times 337.626 / 0.0075 + 1.4 \times 0.005 \times 337.624 / (6.94 \times 10^{-7} \times 10)}{1.4 / 0.0075 + 1.4 \times 0.005 / (6.94 \times 10^{-7} \times 10)}$$

$$= 337.624 \text{ K or } 64.474 \text{ °C}$$

Appendix E Determining of the Density, Specific Heat and Diffusivity of Asphalt Pavement

E.1 Density

The density of the asphalt samples is determined by weighing each sample and calculating the volume from the given dimensions of each sample. The two mix A samples have a diameter of 150 mm and a height of 60 mm, while the two mix B samples have a diameter of 150 mm and a height of 50 mm. The density of the samples are then found by dividing the mass of each sample with its volume.

E.2 Sample Calculation for the Determination of the Density of a Mix A Sample

Measured mass of one of the mix A samples:

$$m_{mix\,A1} = 2.405 \text{ kg}$$

Volume of the mix A samples:

$$V_{mix\,A1} = \frac{\pi D^2}{4} H = \frac{\pi \times 0.15^2}{4} \times 0.06 = 1.060 \times 10^{-3} \text{ m}^3$$

Density of the mix A sample:

$$\rho_{mix\ A1} = \frac{m_{mix\ A1}}{V_{mix\ A1}} = \frac{2.405}{1.060 \times 10^{-3}} = 2268.868 \text{ kg/m}^3$$

The density of all four samples is shown in Table E.1.

Table E.1: Experimental density of the four asphalt samples:

	Mass [kg]	**Volume [m^3]**	**Density [kg/m^3]**
Mix A Sample 1	2.405	1.060×10^{-3}	2268.868
Mix A Sample 2	2.480	1.060×10^{-3}	2339.623
Average	**2.443**	**1.060×10^{-3}**	**2304.245**
Mix B Sample 1	1.980	0.884×10^{-3}	2239.819
Mix B Sample 2	1.960	0.884×10^{-3}	2217.195
Average	**1.970**	**0.884×10^{-3}**	**2228.507**

E.3 Specific Heat

The asphalt pavement sample is ground into small pieces and a known mass $m_{asphalt}$ of pavement at a known temperature $T_{asphalt}$ is mixed with a known amount of hot water m_{water} at a known temperature T_{water} in a vacuum flask. The mixture's equilibrium temperature T_f is measured and the specific heat of the pavement sample is calculated by rearranging the applicable energy equation, i.e.

$$m_{asphalt}c_{p\ asphalt}(T_f - T_{asphalt,\ i}) = m_{water}c_{p\ water}(T_{water,\ i} - T_f) \quad \text{(E.1)}$$

or

$$c_{p\ asphalt} = \frac{m_{water} c_{p\ water} \left(T_{water,\,i} - T_f\right)}{m_{asphalt} \left(T_f - T_{asphalt,\,i}\right)} \tag{E.2}$$

E.4 Sample Calculation for the Determination of the Specific Heat of the Mix A Asphalt Samples

Measured amount of asphalt pavement:

$$m_{asphalt} = 0.137 \text{ kg}$$

Measured initial temperature of the asphalt pavement:

$$T_{asphalt,\,i} = \frac{24.260 + 25.569}{2} = 24.9146 \text{ °C or } 298.065 \text{ K}$$

Measured amount of water:

$$m_{water} = 0.245 \text{ kg}$$

Measured initial temperature of the water:

$$T_{water,\,i} = 59.073 \text{ °C or } 332.223 \text{ K}$$

Measured final mixture temperature:

$$T_f = \frac{55.985 + 54.698 + 54.369}{3} = 55.017 \text{ °C or } 328.167 \text{ K}$$

Specific heat of water at $T_{water,\,i}$ (Kröger (2004)):

$$\begin{aligned} c_{p\ water,\,i} &= 8.15599 \times 10^{3} - 2.80627 \times 10 T_{water} + 5.11283 \times 10^{-2}\ T_{water}^{2} \\ &\quad - 2.17582 \times 10^{-13} T_{water}^{6} \\ &= 8.15599 \times 10^{3} - 2.80627 \times 10(332.223) + 5.11283 \times 10^{-2}\ (332.223)^{2} \\ &\quad - 2.17582 \times 10^{-13} (332.223)^{6} \\ &= 4183.504\ \text{J/kgK} \end{aligned}$$

Specific heat of water at T_f (Kröger (2004)):

$$\begin{aligned} c_{p\ water,\,f} &= 8.15599 \times 10^{3} - 2.80627 \times 10 T_{water} + 5.11283 \times 10^{-2}\ T_{water}^{2} \\ &\quad - 2.17582 \times 10^{-13} T_{water}^{6} \\ &= 8.15599 \times 10^{3} - 2.80627 \times 10(328.167) + 5.11283 \times 10^{-2}\ (328.167)^{2} \\ &\quad - 2.17582 \times 10^{-13} (328.167)^{6} \\ &= 4181.163\ \text{J/kgK} \end{aligned}$$

Specific heat of the mix A asphalt sample using equation (E.2):

$$c_{p\ asphalt} = \frac{0.245\left(4183.504 \times 332.223 - 4181.163 \times 328.167\right)}{0.137\left(328.167 - 298.065\right)} = 1053.705\ \text{J/kgK}$$

Table E.2: Experimental specific heat of the two asphalt pavement mixes.

	Reading number	$m_{asphalt}$ [kg]	$T_{asphalt,\,i}$ [°C]	m_{water} [kg]	$T_{water,\,i}$ [°C]	T_f [°C]	$c_{p\ water,\,i}$ [J/kgK]	$c_{p\ water,\,f}$ [J/kgK]	$c_{p\ asphalt}$ [J/kgK]
Mix A	**1**	0.137	24.915	0.245	59.073	55.017	4183.5	4183.5	1053.7
Mix A	**2**	0.203	28.183	0.325	59.439	55.730	4183.7	4181.5	943.60
Average		**0.170**	**26.549**	**0.285**	**59.256**	**55.374**	**4183.6**	**4181.4**	**998.65**
Mix B	**1**	0.269	24.717	0.467	57.620	54.029	4182.6	4179.5	927.60
Mix B	**2**	0.166	22.579	0.255	60.856	55.956	4184.7	4181.7	988.95
Mix B	**3**	0.224	29.283	0.343	62.884	59.859	4186.0	4180.7	918.29
Average		**0.220**	**25.526**	**0.355**	**60.453**	**56.615**	**4184.4**	**4180.6**	**944.95**

E.5 Sample Calculation for the Determination of the Diffusivity of the Mix A Asphalt Samples

Estimated conductivity for the two mix A samples:

$$k_{mix\,A} = 1.4 \text{ W/mK}$$

Average density of the two mix A samples:

$$\rho_{mix\,A} = 2304.245 \text{ kg/m}^3$$

Average specific heat for the two mix A samples:

$$c_{p\ mix\,A} = 998.65 \text{ J/kgK}$$

Diffusivity of the two mix A samples:

$$\alpha_{mix\,A} = \frac{k}{\rho c_p} = \frac{1.4}{2304.246 \times 998.65} = 6.084 \times 10^{-7} \text{ m}^2/\text{s}$$

Table E.3: Experimental diffusivity of the two asphalt pavement mixes.

	$k_{asphalt}$ [W/mK]	$\rho_{asphalt}$ [kg/m^3]	$c_{p\ asphalt}$ [J/kgK]	$\alpha_{asphalt}$ [m^2/s]
Mix A	1.4	2304.245	998.65	6.084×10^{-7}
Mix B	1.7	2228.507	944.95	8.072×10^{-7}